Part II Dynamic Modeling

Table of Contents

List of Tables

List of Figures

5 Dynamic Modelling

5.1 Dynamic Model Inputs

5.1.1 PVT

5.1.1.1 Input Data

The following PVT-related data was provided

- BGM: Composition and Hall-Yarborough-based computation of gas properties (in the form of an MS Excel sheet);
- GRT: Composition and Hall-Yarborough-based computation of gas properties (in the form of an MS Excel sheet);
- BER: *z* as a function of pressure (in the context of a p/z spreadsheet).

The underlying PVT reports were not available. No information on dew point or condensate was received. As mentioned in chapter 3, no formation water data was received.

5.1.1.2 Processing & QC

The composition data and PVT analysis provided by Taqa, were cross-checked against Hall-Yarborough as implemented in Petrel RE, and as implemented in an Horizon-internal spreadsheet. The Taqa analysis agreed well with the latter, but disagreed with the Petrel RE analysis. The reason for this is unknown, as the Petrel RE documentation does not clearly specify implementation details. Nevertheless, we concluded that we had no reason to doubt that the analysis as per Taqa input was reliable, and we used it in the modelling.

For Bergen no composition data was available. Since the Bergen field was not the main focus of the study, we took a pragmatic approach to this problem: we took the Groet PVT, and adapted the methane content until the z vs. p curve for Bergen matched the one that was used in the Taqa p/z analysis spreadsheet.

As regards condensate, it appears from the production data (see e.g. Figure 5-3, where a CGR vs. time graph is plotted), that condensate ratios are low. However, this is not sufficient to deduce a proper PVT/CGR.

Formation water properties (salinity: salt-saturated) were deduced from apparent Rw values (chapter 3).

Table 5-1 BGM composition (left) and GRT composition (right)

Component	Moles
Nitrogen	0.970
Methane	94.535
Carbon dioxide	0.699
Ethane	3.048
Hydrogen sulfide	0.000
Propane	0.444
i-Butane	0.086
n-Butane	0.079
i-Pentane	0.024
n-Pentane	0.024
Hexanes	0.019
C7+	0.072
Total:	100.000
C7+ Mole Weight	116
C7+ Density, g/cc @ 60F	0.7931
Gas Gravity	0.590
Default C7+ MW	100
Default C7+ Density	0.70

Component	Moles
Nitrogen	2.986
Methane	92.272
Carbon dioxide	1.044
Ethane	2.922
Hydrogen sulfide	0.000
Propane	0.437
i-Butane	0.050
n-Butane	0.085
i-Pentane	0.026
n-Pentane	0.024
Hexanes	0.025
C7+	0.129
Total:	100.000
C7+ Mole Weight	116
C7+ Density, g/cc @ 60F	0.7931
Gas Gravity	0.603
Default C7+ MW	100
Default C7+ Density	0.70

Table 5-2 **Bergen composition as adapted from the Groet composition by decreasing the methane fraction until the z vs. p curve matched the supplied one.**

	GROET	Bergen
Component	Moles	Moles
Nitrogen	2.986	5.023
Methane	92.272	87.000
Carbon dioxide	1.044	1.756
Ethane	2.922	4.915
Hydrogen sulfide	0.000	0.000
Propane	0.437	0.735
i-Butane	0.050	0.084
n-Butane	0.085	0.143
i-Pentane	0.026	0.044
n-Pentane	0.024	0.040
Hexanes	0.025	0.042
C7+	0.129	0.217
Total:	100.000	100.000
C7+ Mole Weight	116	116
C7+ Density, g/cc @ 60F	0.7931	0.7931
Gas Gravity	0.603	0.636
Default C7+ MW	100	100
Default C7+ Density	0.70	0.70

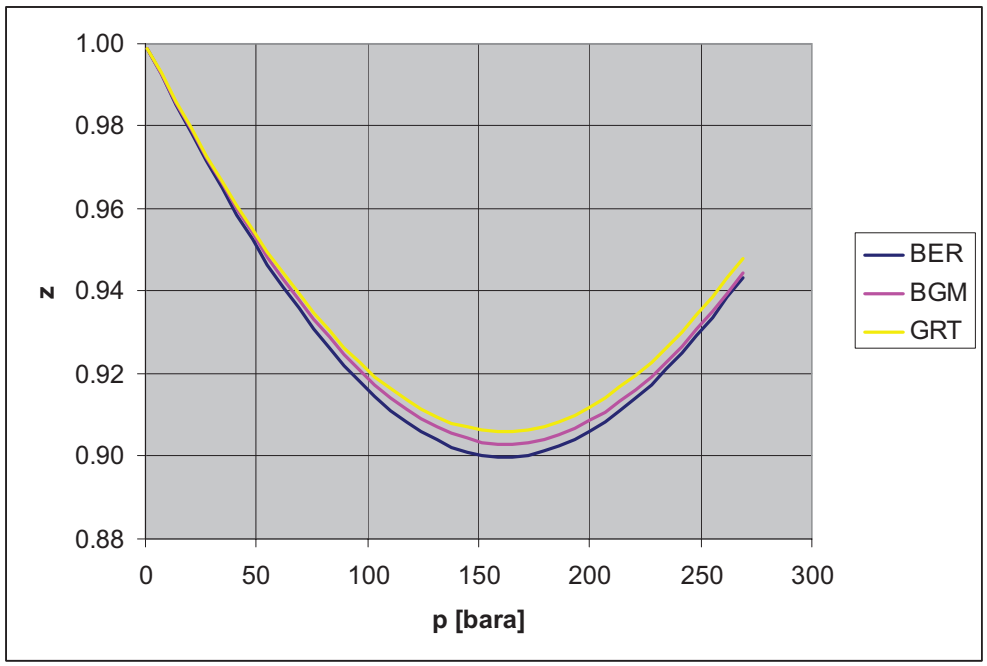

Figure 5-1 Pressure vs. z behavior of the three modelled fields.

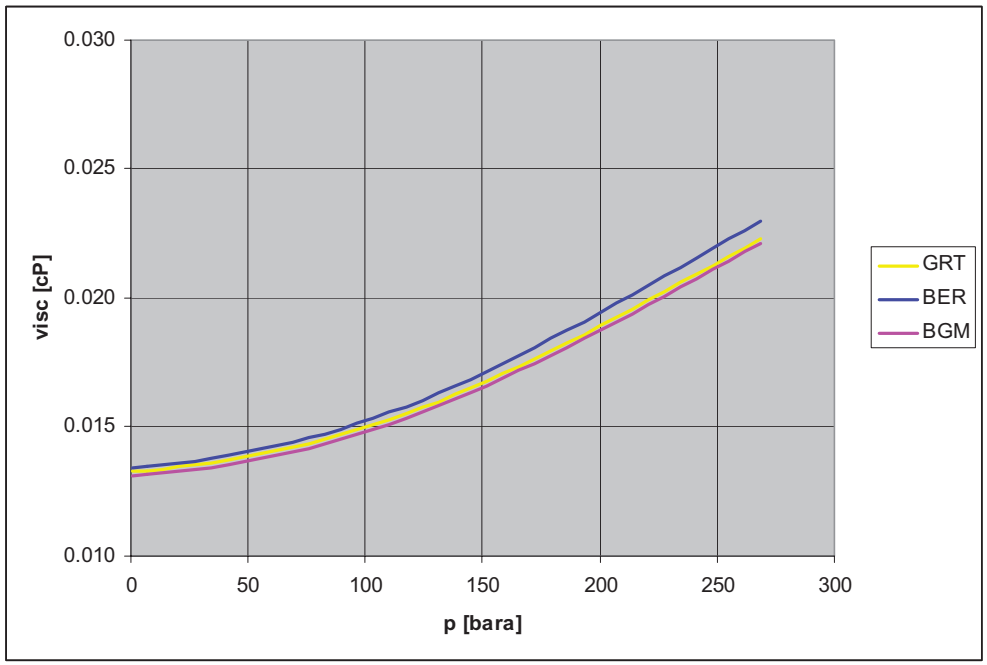

Figure 5-2 Viscosity vs. pressure for the three fields studied.

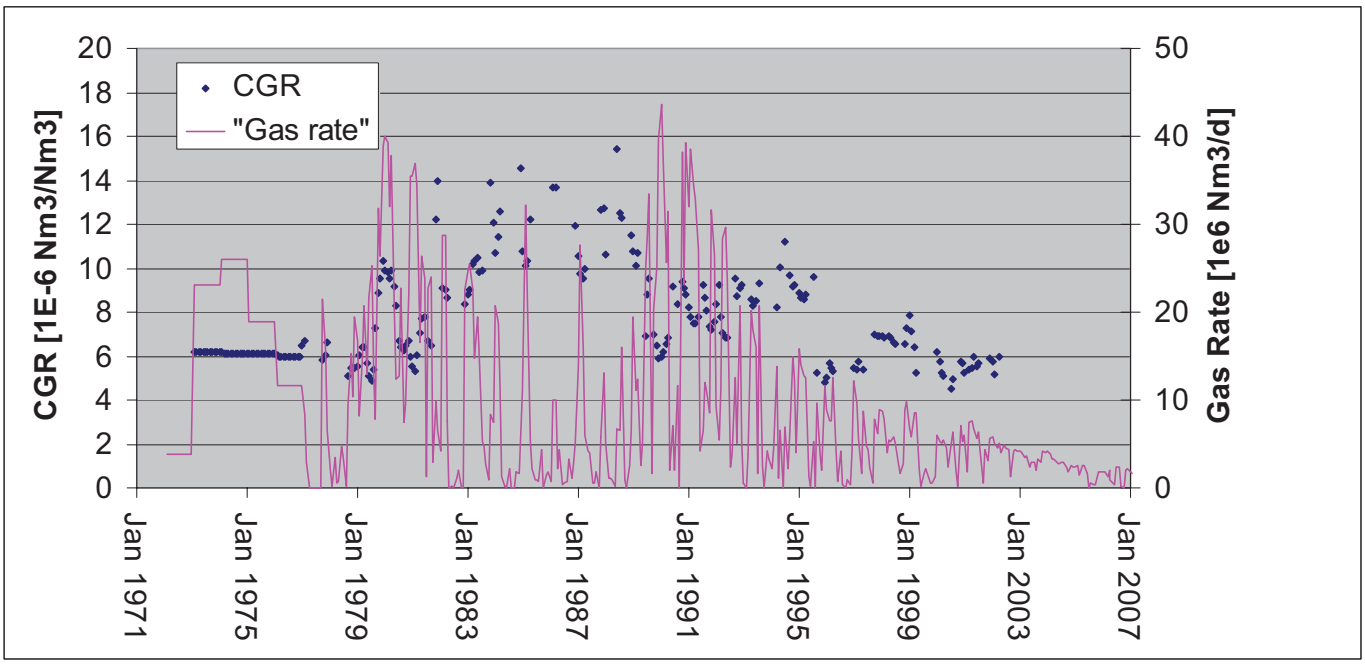

Figure 5-3 Gas rate andR of well BGM1 over time.

5.1.2 SCAL

5.1.2.1 Input data

A report on 'Special Core Analysis; BGM1 and BGM2' was provided [15].

5.1.2.2 Processing & QC

In the SCAL work plug data over a range of depths, in the BGM1 and BGM2 wells, was analyzed. Apart from work relating to petrophysics, relations were investigated between por/perm on the one hand, and trapped gas & water/gas relative permeabilities on the other. Capillary pressure data was also obtained. The main conclusions relevant to this study were:

- Residual (trapped) gas saturation was in essence independent of permeability, although it increased slightly for decreasing permeability
- The samples likely existed in a near neutral state of wettability during low-pressure dynamic displacement of gas by water.
- In the presence of irreducible water, a trend of decreasing relative permeability to water with decreasing air permeability was observed.
- Water saturations at a selected capillary pressure indicated a trend of increasing values with decreasing permeability.
- A dimensionless correlation of water-oil relative permeability may be used with trapped gas and end-point relative permeabilities as reported, to define complete curves of water gas relative permeability for samples of desired permeability.

As regards this latter conclusion, the proposed workflow was replaced by a Corey fit to the data (section 5.3.3).

The capillary pressure measurements done were not used, as in the BGM field (the main focus of the study), the logs indicate a clear contact without transition zone.

No detailed QC of the SCAL work was in the scope of the project. No correction of the oil-based measurements was attempted; sensitivities showed that the relative permeabilities were not a critical uncertainty in either the history match or the forecast UGS behaviour (section 5.3.9.5.2).

It is also important to note that as far as can be ascertained, the SCAL data was not available for the the petrophysical study ([1]; see also chapter 3), the results of which are therefore not necessarily in agreement with these data.

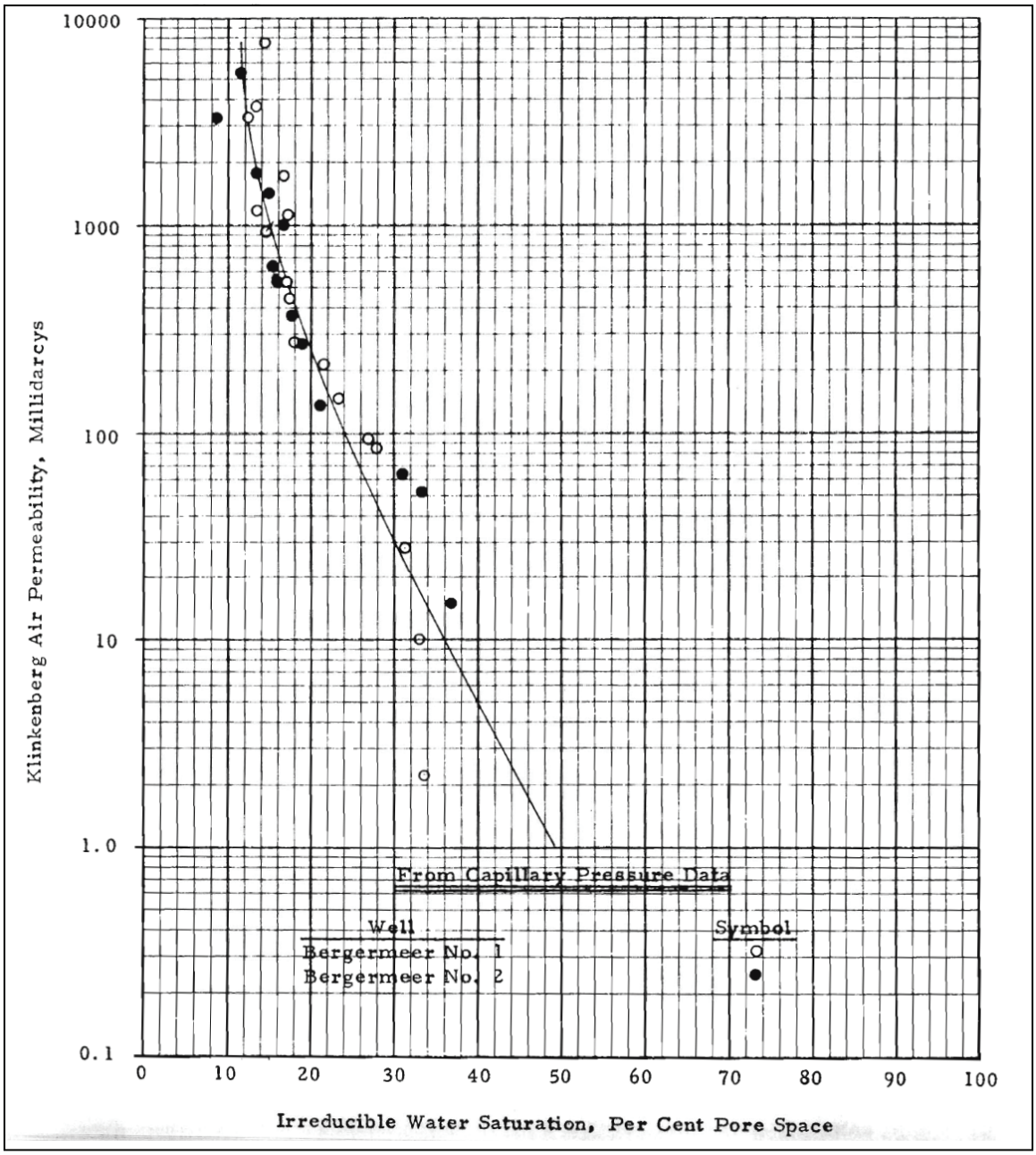

Figure 5-4 Permeability vs Scw.

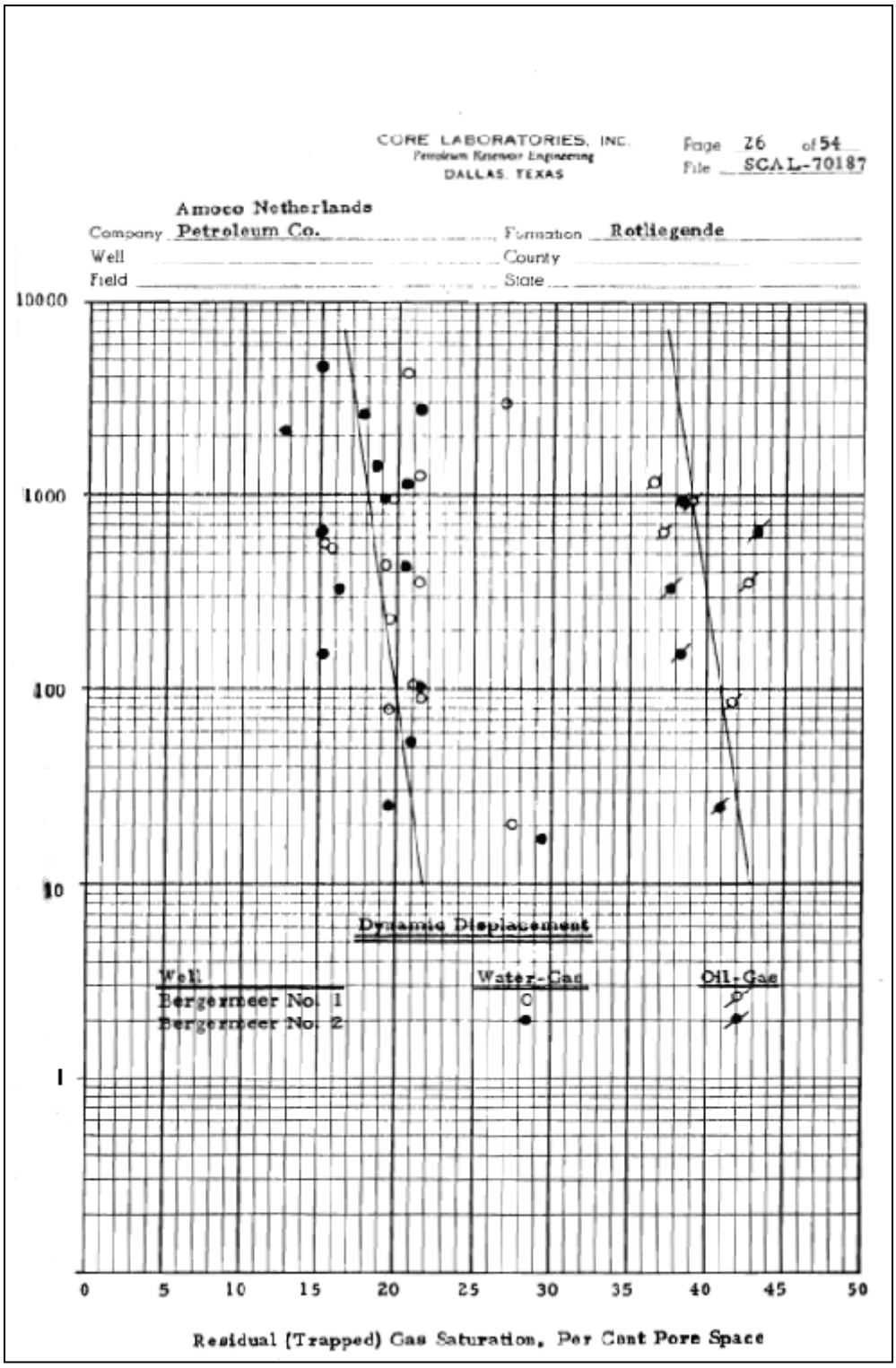

Figure 5-5 Permeability vs Sgr.

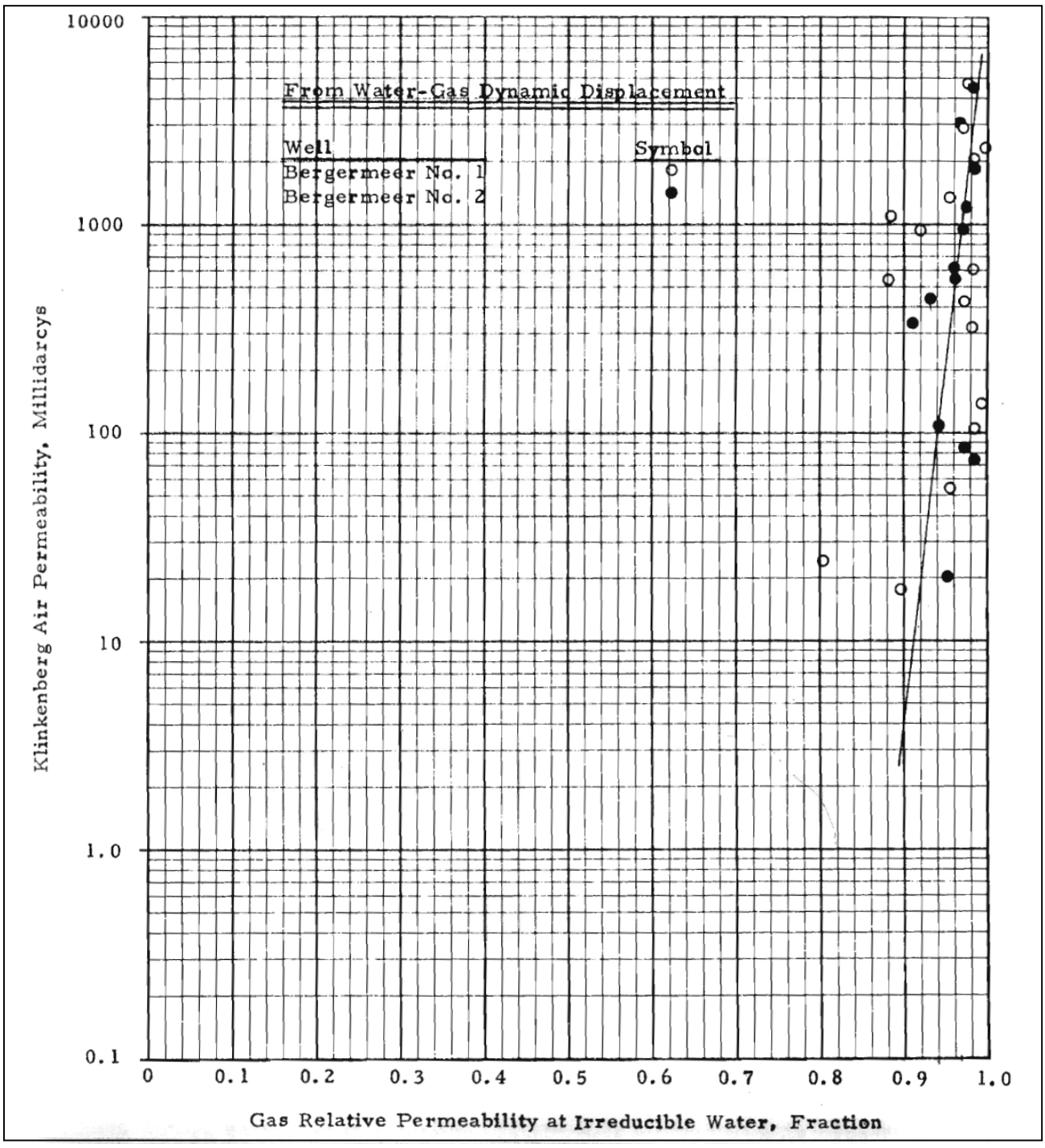

Figure 5-6 **Permeability vs. Krg@Scw.**

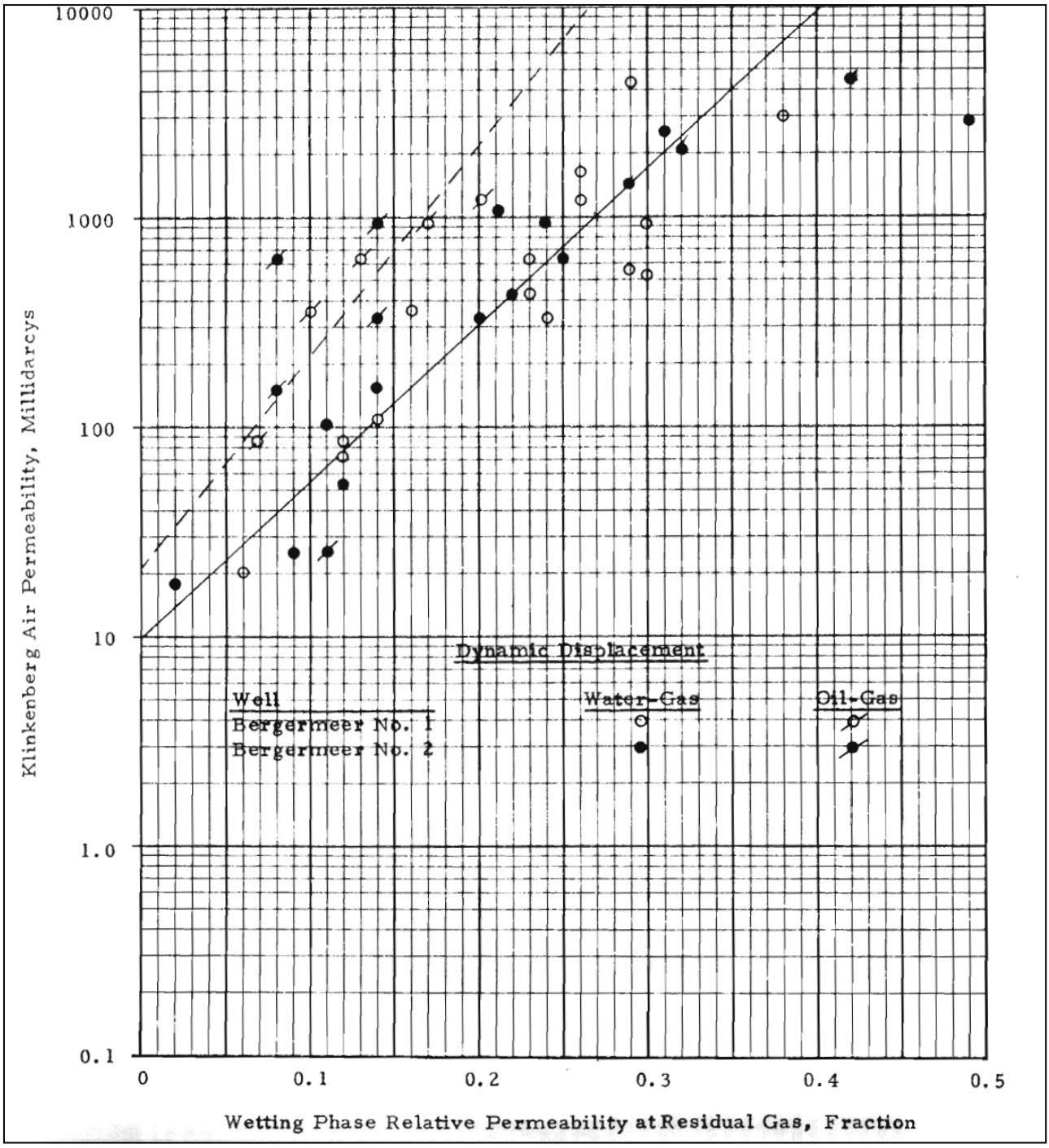

Figure 5-7 **Permeability vs Krw @ Sgr.**

Table 5-3 **Data of the three samples for which full relperm curves are reported.**

Sample	49	37	44
Well	BGM2	BGM1	BGM1
MD [m]	2519.5	2125.3	2095.4
Perm (KL, to air) [mD]	1430	573	73
Oil Perm@ connate water [mD]	1320	491	51
Water Perm @ residual oil [mD]	803	285	25
Por [%]	23.9	21.9	16
Scw [%]	19.5	18.6	25.9
Sor [%]	19	16.7	21.5

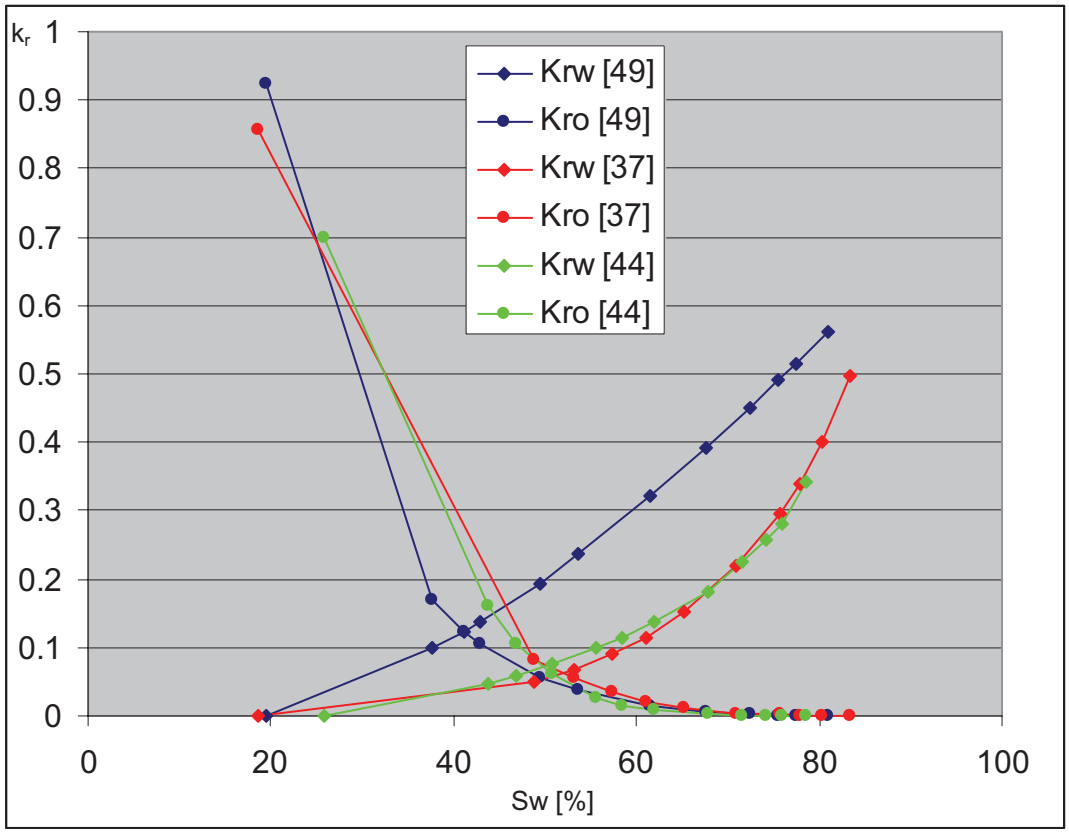

Figure 5-8 **Relperm data measured for the three samples of Table 5-3.**

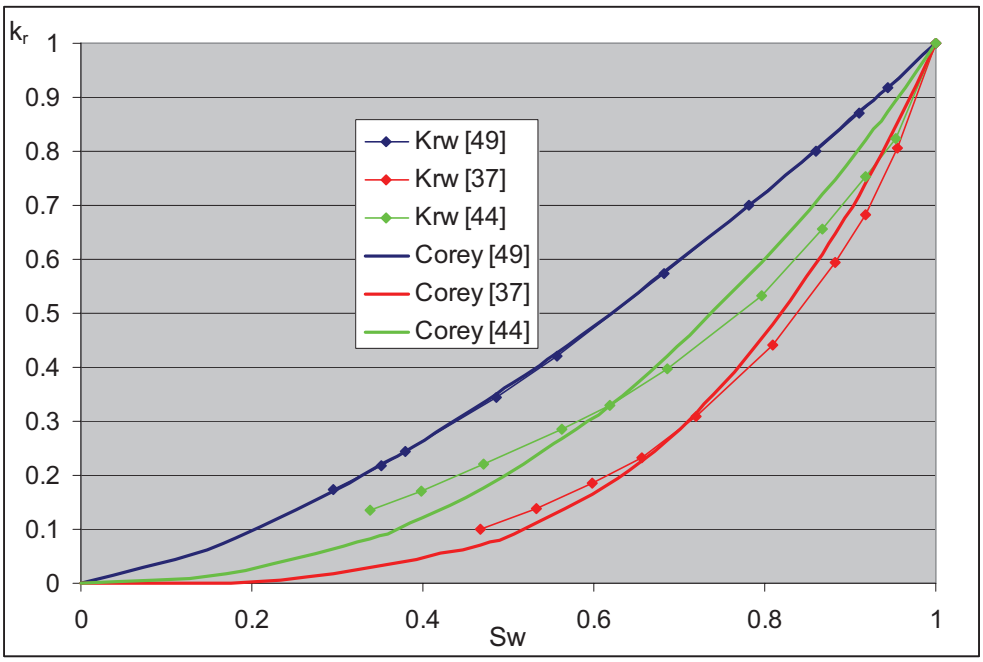

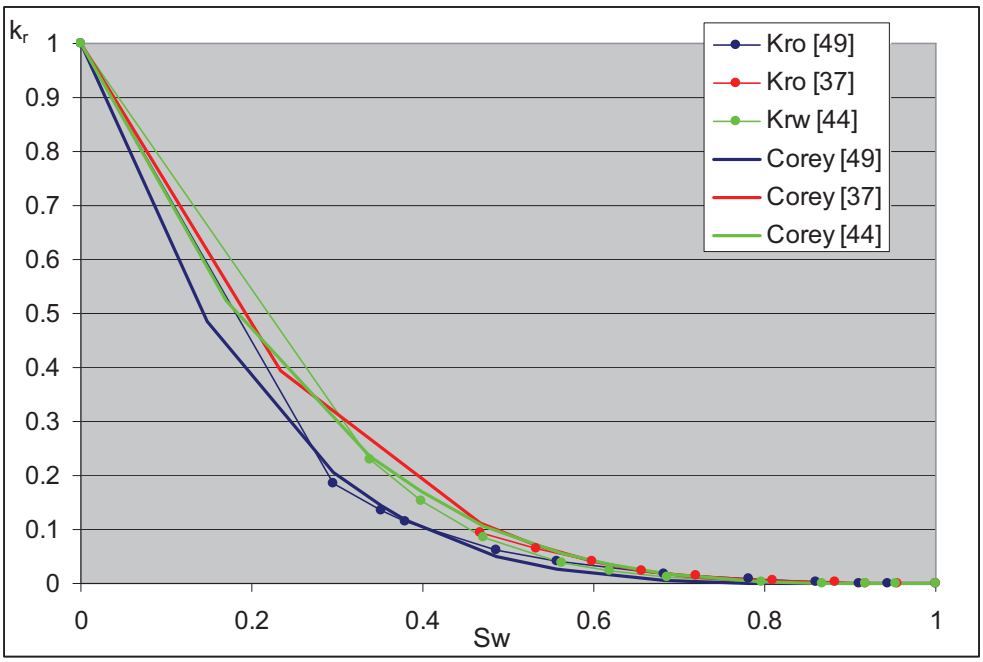

Figure 5-9 **Corey coefficient fits (Table 5-4) to dimensionless relperm data for the three samples (Table 5-3).**

Table 5-4 Corey coefficients from fit (Figure 5-9)

Sample#	Kl air	Corey w	Corey o
49	1430	1.45	4.5
37	573	3.5	3.5
44	73	2.3	3.5

5.1.3 Production & pressure history

The production history was provided by Taqa in the form of an MS Excel spreadsheet. No water production data was available, although some remarks about water production appear in the well (completion) histories (e.g. with BGM3A, where it is related to a cement bond failure). There are some issues with this data, as noted by Taqa:

- BGM: found individual well production from 7701 till 9811. Only field allocated data from 1972 till 1976. Distribute evenly over wells based on production performance. BGM3 was shut in regularly because of water production, not corrected for in this analysis.
- All: Adjusted individual well data for first years (roughly before 1979) to match with November 1998 production report

For the conversion Nm3→Sm3 the factor 1.054915 was used.

Static pressure data was provided in the context of p/z MS Excel spreadsheets for the three fields (Figure 5-17). Build-up and/or gradient data on which the measurements are based was sparsely available (in well test reports; section 5.1.5). No attempt was made to quality-check this data. However, when inspecting them graphically (Figure 5-15, Figure 5-14, Figure 5-16), we can make two observations:

- The GRT data shows significantly more scatter than the BER and BGM data. This could point to lower permeabilities (in line with the observed likely transition zone in GRT).
- The deviations from the straight-line p/z behaviour show similar patterns for the three fields; visually there appears to be a correlation with the rates.

We will discuss these issues in section 5.2.1 in more detail.

5.1.4 Contact Movements

In well BGM1 the GWC has been monitored. The results of these measurements were available (Table 5-5, Figure 5-10).

In addition, wells BGM7 and BGM8 were drilled post-production, and give some information on contact dynamics. It should also be noted that some of the contact rise measurements are after high-rate production periods (i.e. not in the summer); it is not clear whether the water level was given enough time to

settle out before the measurement was carried out [16]. However, the August 2006 measurement confirms the rise to be 20m.

Finally in the completion (well) history, (an unquantified amount of) water production is reported for BGM3A, which was (partly?) related to poor cement bond.

For the GRT field there is some information that the water table has risen by about 50m over its production period (Table 5-6; viz. the need to recomplete wells upwards). A TDT run during the course of the present project in GRT1 failed to give a conclusive result.

No contact movement data for Bergen was available.

Table 5-5 GWC movement in well BGM. Measurements are from TDT unless stated otherwise.

BGM1					BGM7		
Year / Month	GWC	Rise	Comment		Year / Month	GWC	Comment
	(m TVDSS)	(m)					
Aug-1969	2228.0	0.0	OH		Oct-1981	2231	OH
Jul-1973	2228.0	0.0			Jun-1989	2223.5	Well History?
Jun-1974	2227.6	0.4					
Jul-1975	2226.6	1.4					
Sep-1976	2226.2	1.8					
May-1977	2225.8	2.2					
Jul-1978	2224.8	3.2					
Jul-1979	2224.0	4.0					
Jun-1980	2223.0	5.0					
Jul-1981	2222.8	5.2					
Jun-1982	2222.6	5.4					
Sep-1983	2222.2	5.8					
Sep-1986	2221.4	6.6					
Jun-1989	2221.4	6.6					
Jul-1990	2220.6	7.4					
Dec-1992	2217.5	10.5					
May-1996	2214.5	13.5					
Aug-2006	2207.0	21.0					

Table 5-6 GWC rise in GRT6

DATE	m MDRKB	m TVDSS	Source
Jun-1971	2429	2222.5	Well History/NLL
Mar-1975	2429	2222.5	Well History/NLL(TDT)
Aug-1981	2423	2216.5	Well History/NLL
Sep-1999	2367	2161	Well History/Pulsed Neutron
Sep-2000	2364	2158	Well History/Downhole video

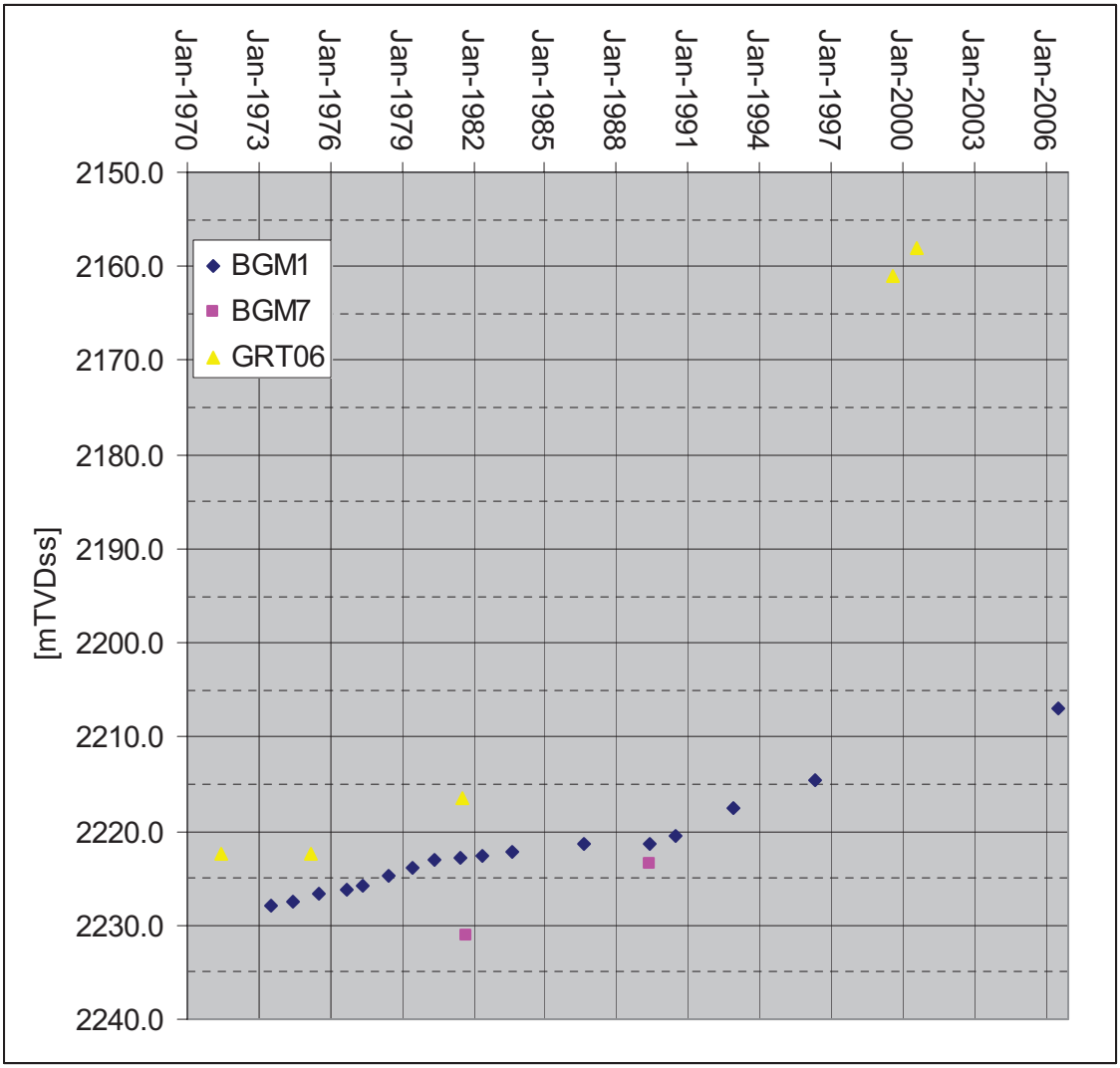

Figure 5-10 Graph of GWC vs. time as observed in BGM1, 7 and GRT6. The initial contacts for GRT and BGM are assumed to be 2217 and 2227, respectively.

5.1.5 Well Test data

The data of a significant number of well tests was available in paper form. No well tests in digital form were available initially. Of some of the older well tests, build-up data was available in graphical form (paper charts), for a few the pressure gauge data in tabular form was found, not all of these complete with rate data. In most well tests the results were analyzed in terms of the overall well performance, relating Q to $(P^2-P_{wf}^2)$. To fully make use of this database would have required a significant amount of work in digitization and QC'ing of this data. Given the time frame of the project, this did not appear feasible.

However, at a late stage of the project, well test data for several wells did arrive. A number of these, where

both pressure and rate data could be found, were analyzed c.q. the pre-existing Taqa analysis was QC'd.

Table 5-7 List of well tests analyzed

Date	Well	# Build-ups	Rates
1986	BGM1	4	2.6e5 - 9.2e5 m3/d
Sept. 1987	BGM1	4	8.5 – 32e6 scf/d
July 1990	BGM1	4	5e5-1e6 m3/d
1987	BGM6	5	10-29e6 scf/d

Table 5-8 Sample KH values from well tests, taken from the headers of well (competion) histories. See section 5.4. In addition to recompletions, the PI is influenced by stimulation jobs & other effects, so is time-dependent.
It should be noted that it is not clear what the 'h' factor in the kh refers to in this case. In view of partial penetration and high kv, it could refer to the full height of the gas zone (which is also variable due to contact movement). However, e.g. the BGM1 history quotes a kh of 182100 mDarcy ft, at permeabilities 'greater than 1 Darcy', which does not match an identification of h with the gas leg height (which is about 150m in this location).
Wells BGM4 and BGM9 are not drilled in the BGM field proper. See 5.4 for more detailed analysis.

[deleted text because of confidentiality]

Well	kh [mD ft]	S	Date	Comment
BGM1	XXX	XXX	XXX	XXX
BGM2	XXX	XXX	XXX	XXX
BMG3A	XXX	XXX	XXX	XXX
BGM5	XXX	XXX	XXX	XXX
BMG6A	XXX	XXX	XXX	XXX
BGM7	XXX	XXX	XXX	XXX
BMG8	XXX	XXX	XXX	XXX

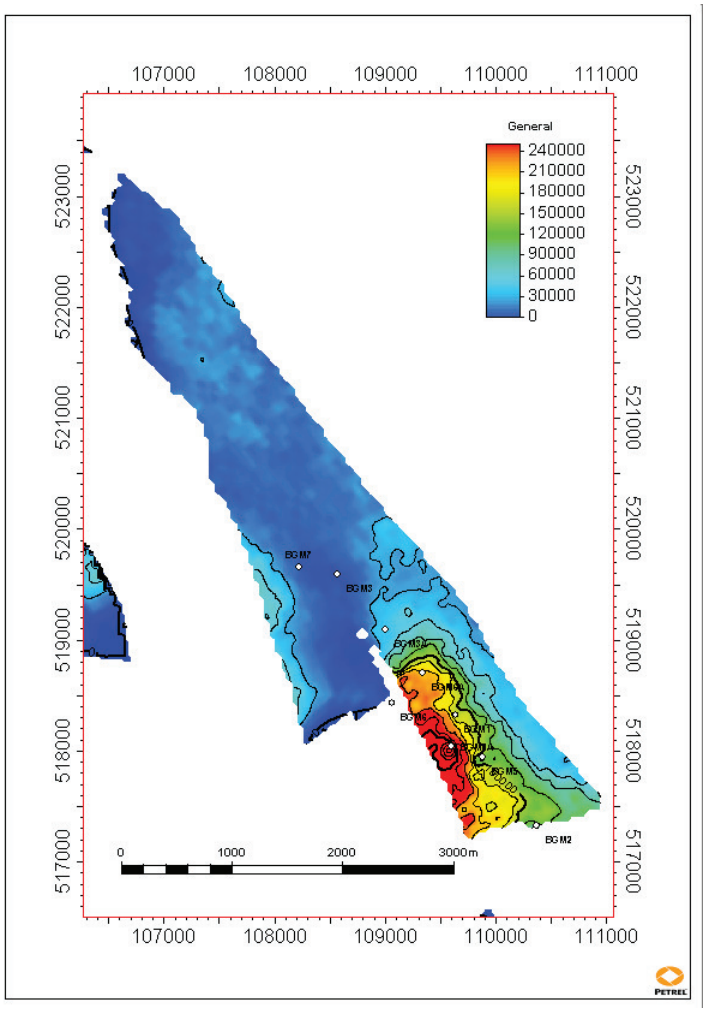

Figure 5-11 Kh distribution in the BGM field [mDarcy m]. The data plotted is based on the 'cont_mid' scenario. The value is the average pre-upscaled permeability over the part of the Rotliegend above the original GWC, multiplied by the distance of the original GWC to the top Rotliegend. The resulting pattern is a reflection of the relief of the structure above the GWC, enhanced by the fact that the permeabilities decrease towards the top of the Rotliegend. The effect is quite dramatic, indicating a fairly well-constrained area of high productivity.

[deleted text because of confidentiality]

Figure 5-12 **KH values extracted from Figure 5-11 vs. KH values from well tests. The line plotted is @ y=x. Although the values in the simulation are too high [the extraction method is simplistic; viz. section 5.4], the general trend matches the observations very well. Thus the contact-to-topROSLU offset, in combination with the 'bell' permeability profile is clearly indicative of the relative well performance.**

5.1.6 Well & Completion data

Completion history files were provided by Taqa (in MS Word and PowerPoint format) for all wells in the three fields. These contain information on (re)perforations, squeezes, stimulations. As mentioned earlier, also some comments on contacts and well performance are made.

5.1.7 Other data

No specific rock mechanical (compaction) data was available.

No RFT data was available for the study.

No PLT data was available for the study (although well (completion) histories do suggest that such measurements were made).

5.2 Material balance

5.2.1 P/z analysis

Figure 5-15, Figure 5-14, Figure 5-16 show the p/z behaviour of the three fields. The data is plotted detrended (i.e. we subtracted a linear p/z vs. cumprod trend from the p/z values) to highlight deviations

from the linear behaviour more clearly (compare Figure 5-13 with Figure 5-14). We can then see that the Bergen field has the straightest behaviour: all points are within 2 bars of the line. In GRT and BGM the spread is more, up to 5 bars.

In the GRT field we can see that the scatter of the points is larger than in BER and BGM. Possibly the pressures in GRT4 and GRT3A are somewhat (1-2 bar) higher than those in GRT1 and GRT6.

In the BGM field we can clearly distinguish the fact that BGM7 exhibits different pressure behaviour. The pressure difference between BGM7 and the main BGM compartment is up to 20 bars, a similar order of magnitude as the pressure differences between GRT and BGM.

Generally, all three fields show pressures initially below the straight p/z line, thereafter above, finally bending back down. The magnitude of the deviation of the curves certainly rules out a strong aquifer. This issue will be addressed in more detail later.

Similarly, there is little evidence of any communication between the fields. In particular for Bergen, with its very straight p/z behaviour, and a pressure difference of up to 50 bars with the other fields (Figure 5-17), this conclusion appears quite solid. For Groet, the scatter in the data could leave some (small) room for inter-field communication, as does the BGM/BGM7 behaviour. As BGM would be re-pressurized, the BGM→GRT pressure differential would grow. Thus the fluxes in the UGS period could conceivably be more significant than in the production period. To address this issue, we will analyze combined BGM/GRT simulation runs later in this chapter.

What is puzzling then, is the very significant contact rises (discussed above) on the one hand, and the lack of evidence in the pressure data for any aquifer on the other. This issue will be examined in the simulation section below.

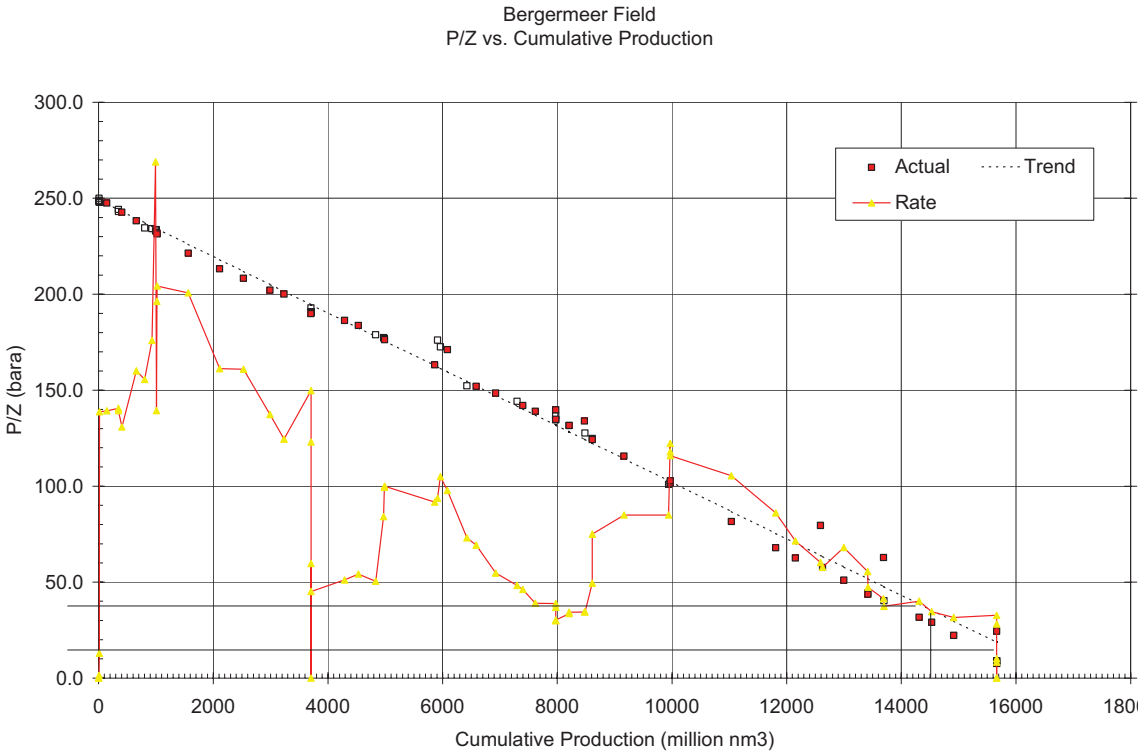

Figure 5-13 **P/z analysis for Bergermeer, overlayed with linear trend and rates [vertical scale for rates is 0-6e6 Nm^3/d]. The pressure points clearly above the trend are from BGM7. Cf. Figure 5-14.**

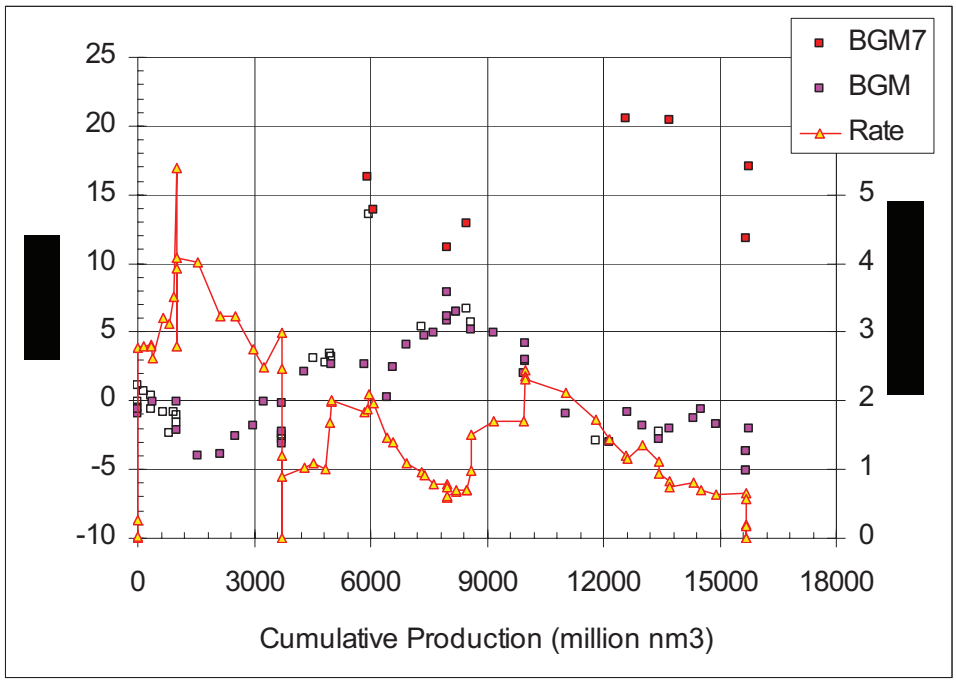

Figure 5-14 Plot of p/z and rate of Bergermeer (Rotliegend) vs. cumulative production. The p/z (Figure 5-13) is detrended with an initial p/z of 249 bar and a GIIP of 16400 Nm3. This allows a better discrimination of deviations from straight-line behavior. Pressures for BGM7 are shown separately, indicating a pressure differential of up to 20 bar.

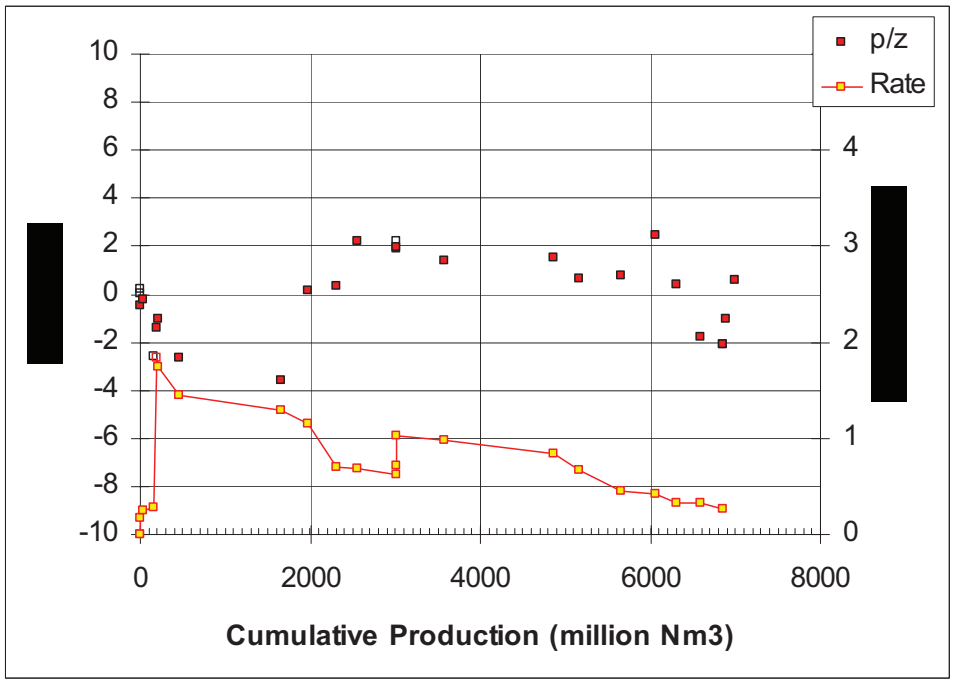

Figure 5-15 Plot of p/z and rate of Bergen (Rotliegend) vs. cumulative production. The p/z is detrended with an initial p/z of 239 bar and a GIIP of 7400 Nm3.

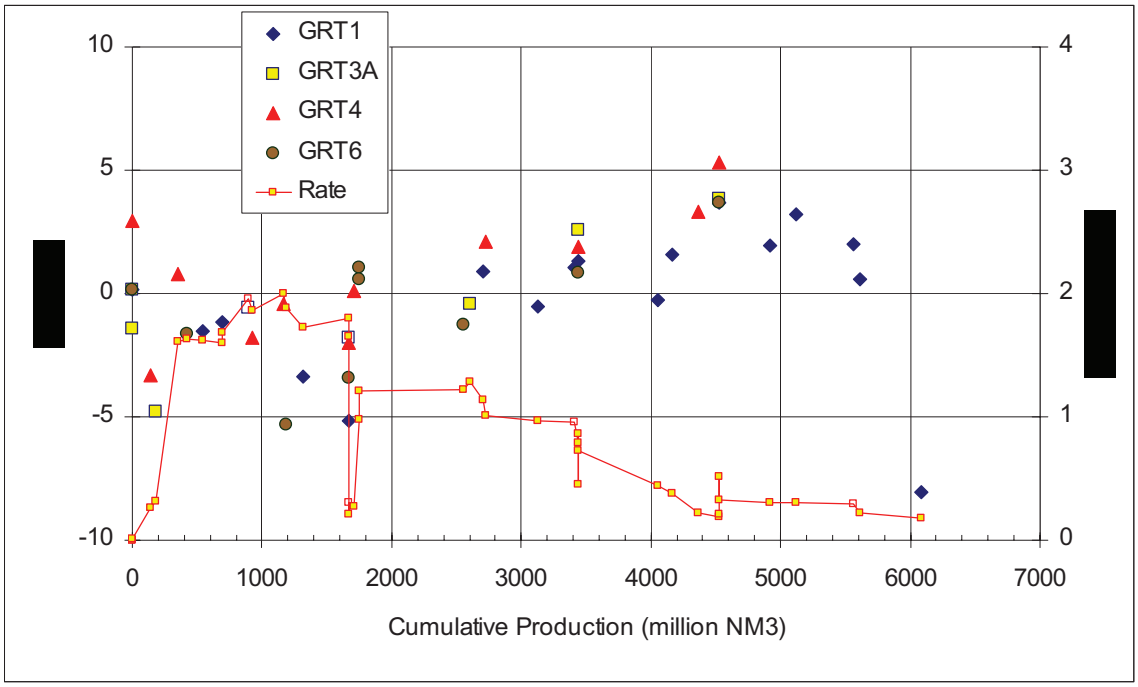

Figure 5-16 Plot of p/z and rate of Groet (Rotliegend) vs. cumulative production. The p/z is detrended with an initial p/z of 249 bar and a GIIP of 7000 Nm3.

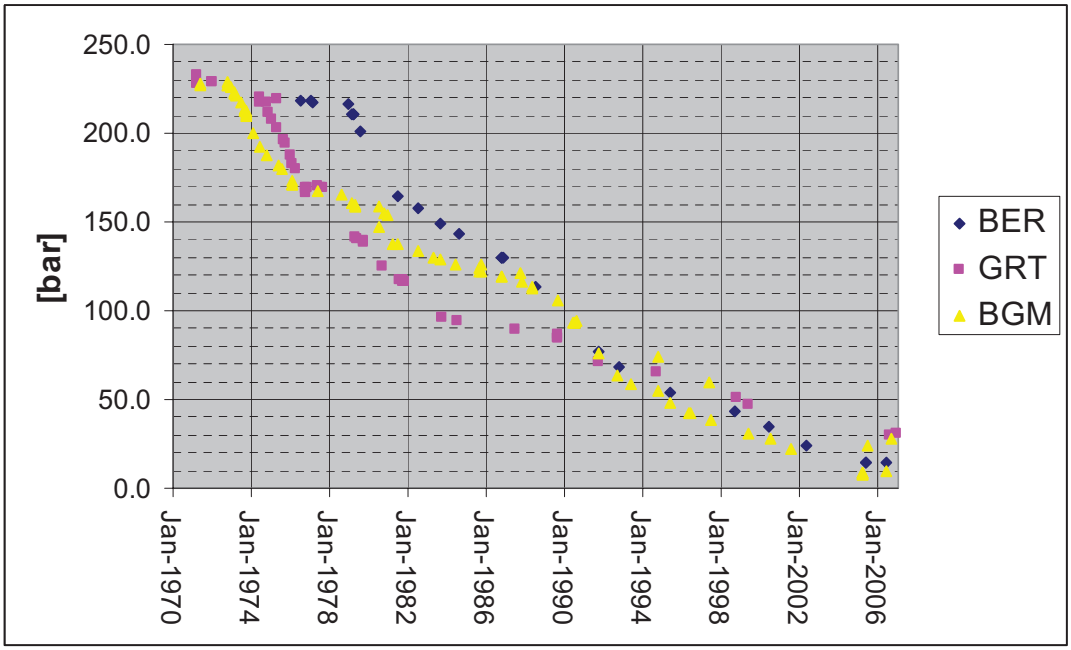

Figure 5-17 Pressure history of the three fields vs. time. Bergen has seen pressures 50 bars higher than Groet and Bergermeer. Groet pressures have been on either side of Bergermeer pressures.

5.2.2 Material balance modelling

After p/z analysis, the next step in modelling is material balance. This should confirm the p/z conclusions more quantitatively, in particular w.r.t. the constraints which the observations put on inter-field communication and aquifer support. In addition, it will shed light on the relative sizes of the BGM7/BGM compartments whose presence we conclude from the pressure data.

The material balance modelling was done in the software package 'MBAL'.

The model consists of 4 tanks, GRT, BER and the two BGM compartments. The production history of each well of Bergermeer was input in the model; Bergen and Groet reservoirs history were modelled via tank history for simplicity. To achieve the objective of the model (assess limits on transmissibilities), 4 transmissibilities were then specified: one between, Bergermeer_main and Bergermeer_7, one between Groet and Bergermeer_main another one between Bergen and Bergermeer_main and a last one between Groet and Bergen. Potential aquifers were added to all the tanks (these were Carter-Tracy-tye aquifers, but this choice is not really material). Figure 5-18 shows the setup of the model.

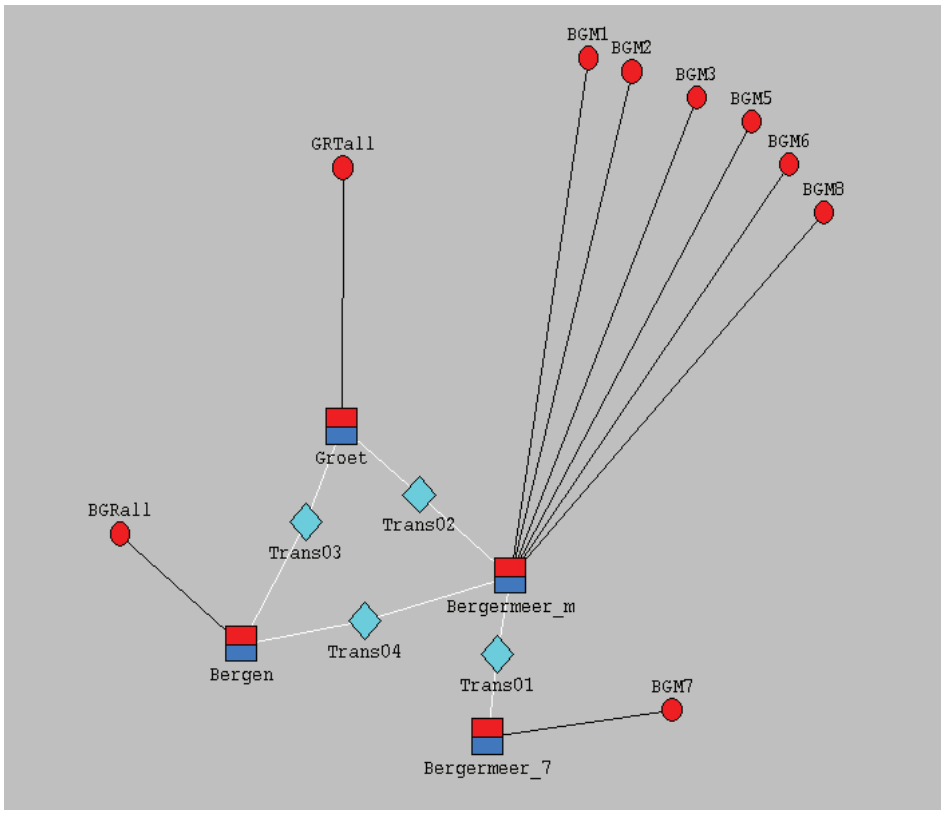

Figure 5-18 Schematic setup of the material balance model.

5.2.2.1 Parameters

The PVT was simplified; we used a common PVT for all reservoirs. The other parameters were specific to each reservoir and are summarized in the following tables. We did not attempt contact matches with MBAL (the reason for this is that, as will become clear in section 5.3.8.2, the contact cannot be assumed to be flat), so porosity and S_w values are not material.

Table 5-9 MBal tank property overview.

	Bergermeer_main	Bergermeer_7	Bergen	Groet
Temperature (deg C)	86.1	86.1	86.1	86.1
Initial Pressure (bara)	227	227	218	226
Porosity	0.21	0.21	0.17	0.21
Connate Water Saturation	0.2	0.2	0.2	0.2
Start of Production (m/d/y)	06/01/1971	07/21/1980	12/07/1978	05/29/1974
Rock compressibility (1/bar)	3E-5	3E-5	3E-5	3E-5

The relative permeabilities were obtained by using notional Corey Functions. [The exponent values differ from section 5.3.3, since the SCAL data was analyzed after the MBAL work was done. Again, since no contact match was attempted, the difference is not significant.]

Table 5-10 MBal tank relperm overview.

	Residual Saturation	End point	Exponent
Krw	0.2	0.9	1.5
Krg	0.19	0.9	1.7

5.2.2.2 Base Match Results

The results of the matching are shown below (Table 5-11). Bergermeer_main and Bergermeer_7 have a total gas in place equal to 18.3 GSm^3 or 17.34 GNm^3 which is close the to the previous analysis made in 1994 [17], in which the GIIP was calculated to be equal to 17.4 GNm^3. [Please note that the volumes reported by MBal, like those in Eclipse, are in Sm^3 rather than Nm^3.]

The match was based on the comparison of the historical pressures and simulated pressures (Figure 5-19, Figure 5-20, Figure 5-21, Figure 5-22). Figure 5-19 shows that the late pressure history is imperfectly matched, but no combination could be found to get a better result while keeping a good pressure match for the other reservoirs.

Table 5-11 **MBal base match results overview. Volumetrics for the simulation model (which will be discussed later) can be found Table 7-5. The trends plotted in Figure 5-14, Figure 5-15, Figure 5-16 show 17.3, 7.8 and 7.4 GSm^3 for BGM, BER and GRT, respectively. The discrepancy for BGM is related to the Bergermeer_7 volume: the higher we assume this volume is, the more gas is left in place @ 2007 (because the block is overpressured), the higher the GIIP must have been. In the p/z plot analysis this effect is neglected.**

GIIP:

	Bergermeer_main	Bergermeer_7	Bergen	Groet
GIIP (GSm^3)	11.3	7	8.08	7.28

Aquifers:

	Bergermeer_main	Bergermeer_7	Bergen	Groet
Reservoir thickness (m)	150	150	150	150
Reservoir radius (m)	2000	1000	1000	1000
Outer/Inner Radius ratio	1	1	1	1
Encroachment Angle	180	180	180	180
Aquifer permeability (md)	1	100	100	100

Transmissibility:

	Bergermeer_main to Bergermeer_7	Bergermeer_main to Groet	Bergermeer_main to Bergen	Groet to Bergen
C (m^3/day*mPa.s/bar)	10	0	0	0.17

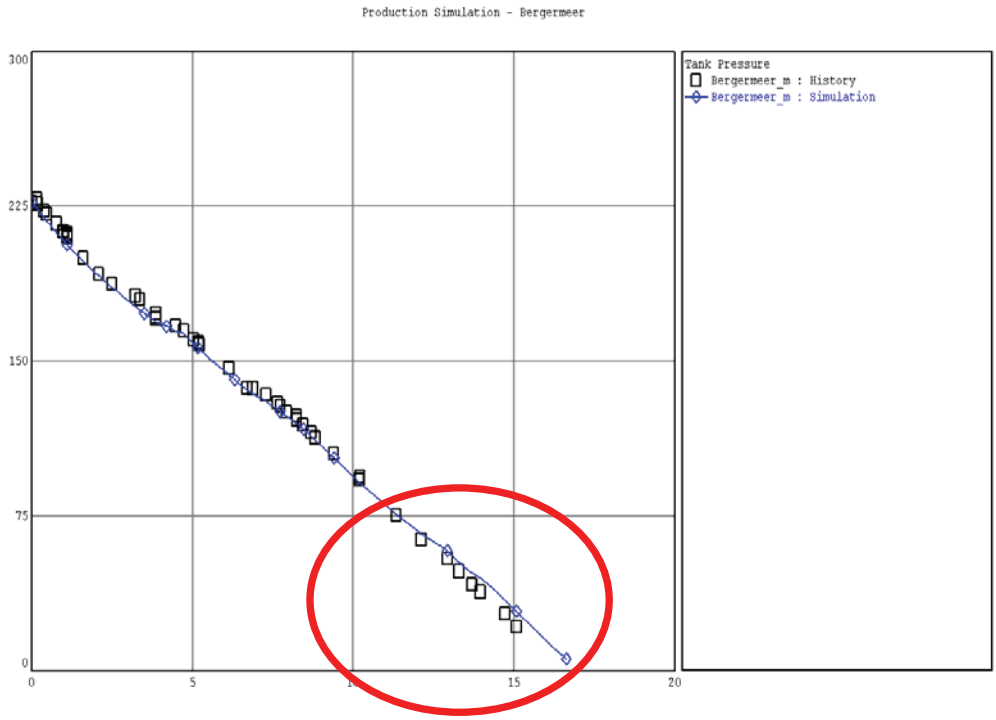

Figure 5-19: **Bergermeer_main pressure match. The red circle indicates the imperfect late pressure match.**

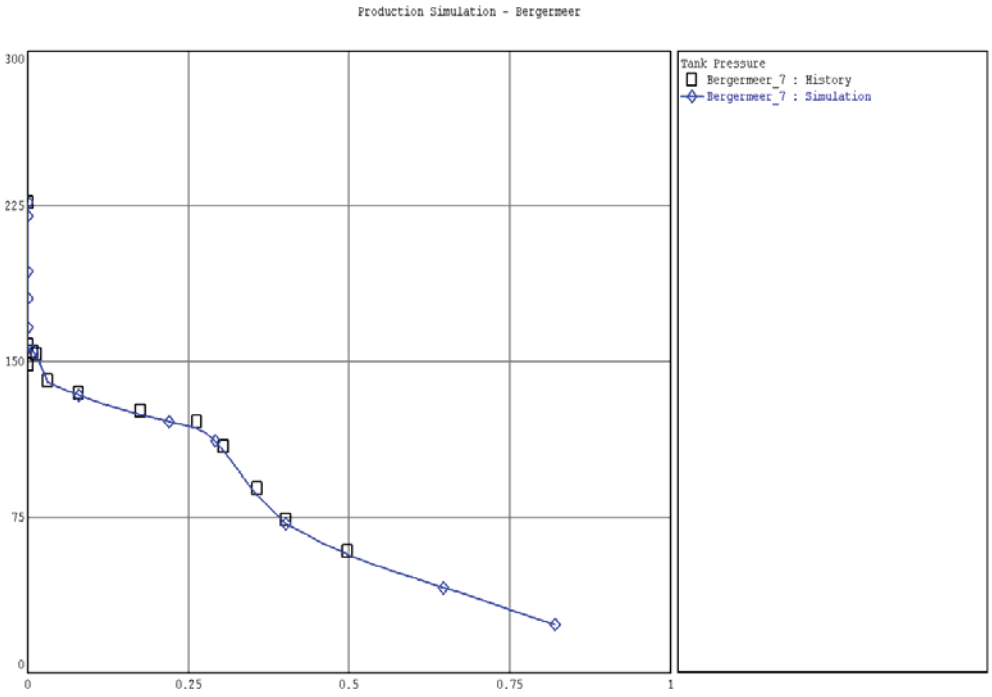

Figure 5-20 **Bergermeer_7 pressure match.**

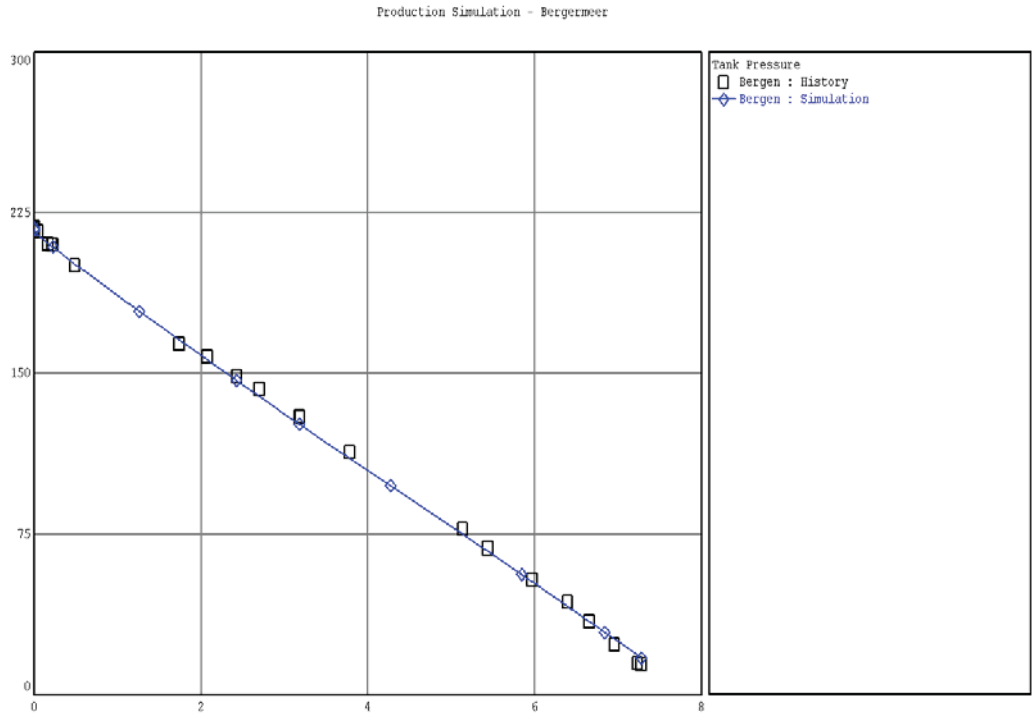

Figure 5-21 Bergen pressure match.

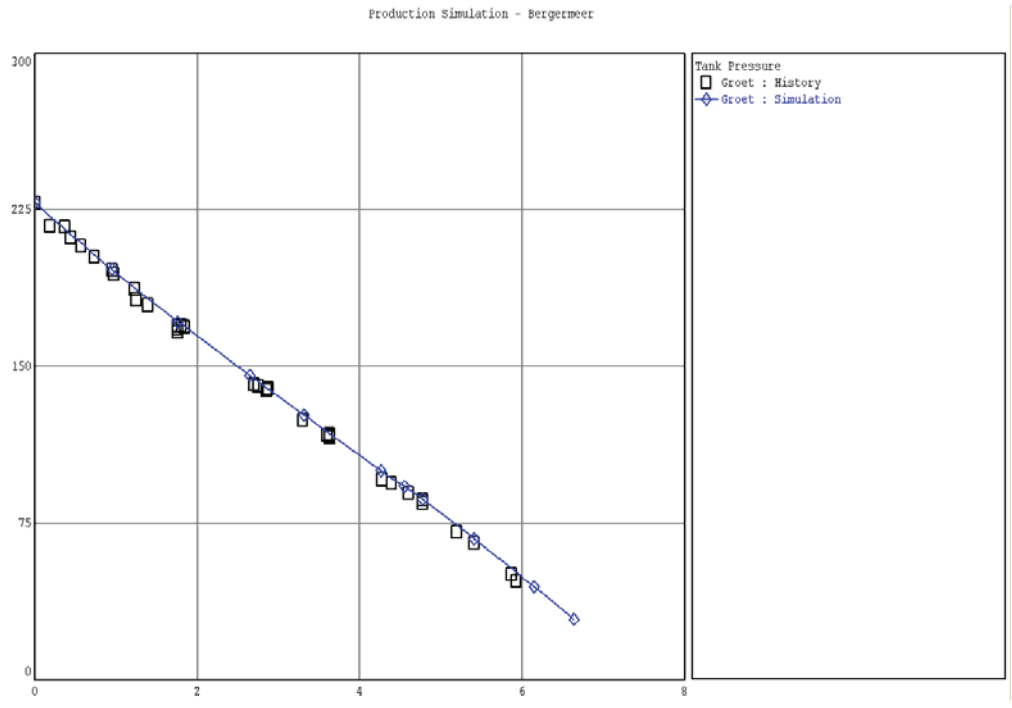

Figure 5-22 Groet pressure match

5.2.2.3 Sensitivities

Several sensitivities have been made on the following properties: transmissibility, aquifer strength and

initial gas in place.

5.2.2.3.1 BGM7 vs. BGM-main GIIP

The volume in Bergermeer_7 is not certain as the seismic does not show a fault fully separating it from Bergermeer_main. A westward extension of 'fault2' leads to quite low volumes for this compartment (chapter 4). If we reduce the gas in place down to 2 GSm^3 and in the same time increased the gas initially in place in Bergermeer_main up to 16 GSm^3 (keeping the total GIIP constant), we need to change the transmissibility was changed from 10 to 2 m^3/day*mPa.s/bar to maintain an approximate match. Figure 5-23 shows the effect of the change on Bergermeer_7. As a result of the lower GIIP, we overpredict the early pressure drop in BGM7. Given our choice to keep the midpoint of the early BGM7 decline matched, we thus overpredict the initial BGM7 pressure, and underpredict the later BGM7 pressure. (We also need to bear in mind that the Bergermeer_7 compartment looses gas through the fault in addition to the production of BGM7.) The effects are reasonably subtle (the difference appears small compared to the symbol size that MBal plots), but is significant. The conclusion is that a 2 GSm^3 volume is too small.

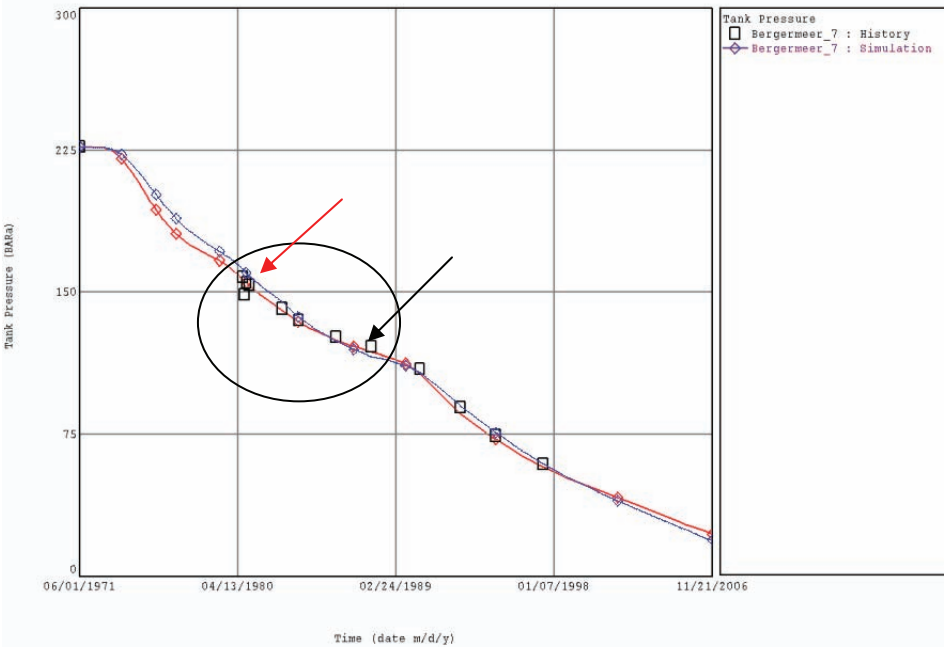

Figure 5-23 Effect of a lower Bergemeer_7 volume on the Bergermeer_7 pressure match (red: base match; blue: low-case Bergemeer_7 volume match). The low-case match shows more rapid pressure decline after BGM7 starts producing (circled). If we tune the model such that we end up at roughly the right pressure at the end of this initial period (black arrow) we will get a too-high pressure at the start of production (red arrow).

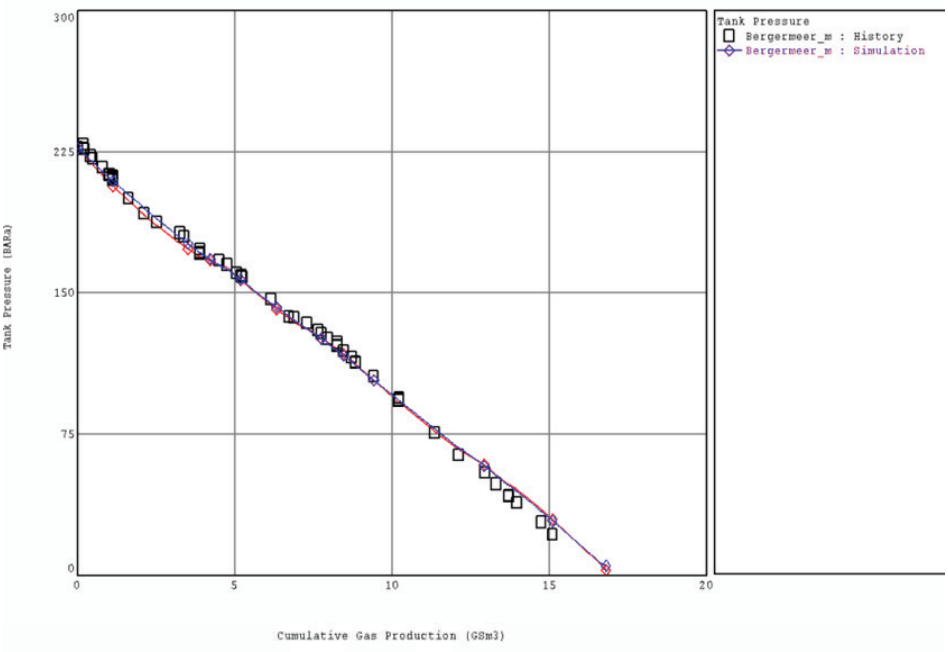

Figure 5-24 Effect of a lower Bergemeer_7 volume on the Bergermeer_main pressure match (red: base match; blue: low-case Bergemeer_7 volume match).

5.2.2.3.2 BGM7 vs. BGM-main GIIP and aquifer

As can be seen from the pressure history of Bergermeer (Figure 5-15), the Bergermeer_7 block has for several reasons (higher final pressure, scarcer data) more room to attach an aquifer; the main block does not show any evidence of additional pressure support. Hence we ran a sensitivity were a non-negligable aquifer was attached to Bergermeer_7 (the GIIP was lowered slightly to keep a pressure match). The transmissibility was increased to 5 to get a better match in the early time (i.e. the pressure support the aquifer gives to BGM7 has to be compensated by additional flow to BGM-main). The green line in Figure 5-25 shows the result of this test.

If the aquifer is too big, too much gas is produced out of Bergermeer_7 in the late time (relative to its GIIP) and then the pressure falls too low. This indicates that the aquifer does not give a big support to the system.

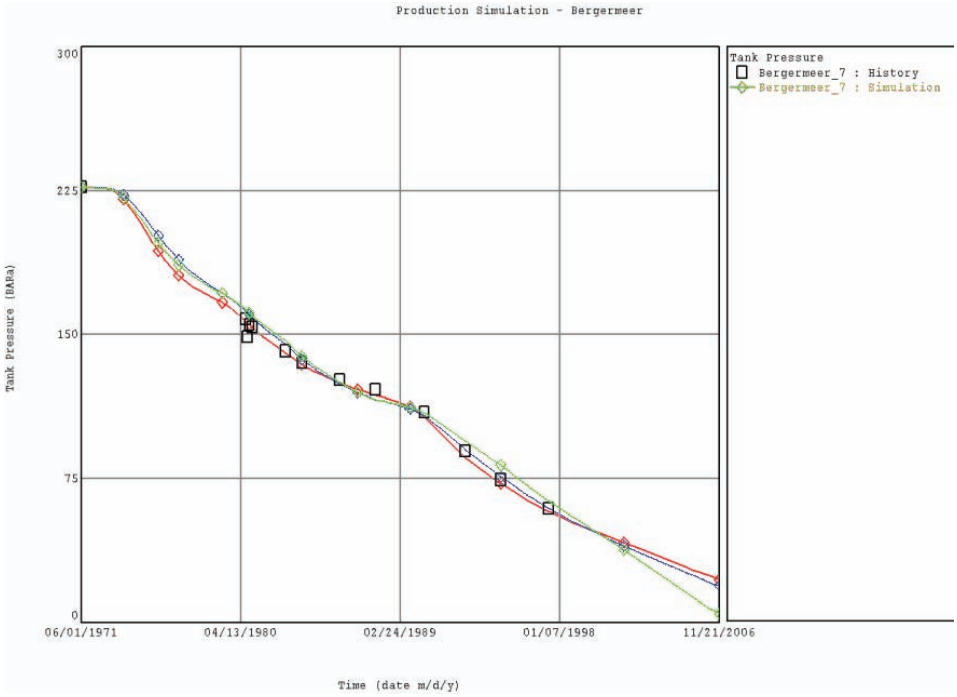

Figure 5-25 Effect of runs with aquifer attached to Bergermeer_7 on the Bergermeer_7 pressures. Red: base, blue: aquifer, green: aquifer+transmissibility increase.

5.2.2.3.3 Inter-field transmissibility

In the base case, we had a fairly small transmissibility from Groet and/or Bergen to Bergermeer. However, if the fault separating the two BGM compartments runs east, rather than west, the northern part of the Beregrmeer field is in the Bergermeer_7 compartment. Since the connection to the other fields is here, in this scenario these other fields to Bergermeer_7 rather than the main compartment. For the same reasons as above, this could offer more room to achieve a match with increased transmissibilities. Figure 5-26 shows the modified set up. The pressure match of Bergermeer_main is shown in Figure 5-27.

New GIIP distributions are shown below; the differences are not so large that the MBal analysis can decide which scenario is more likely.

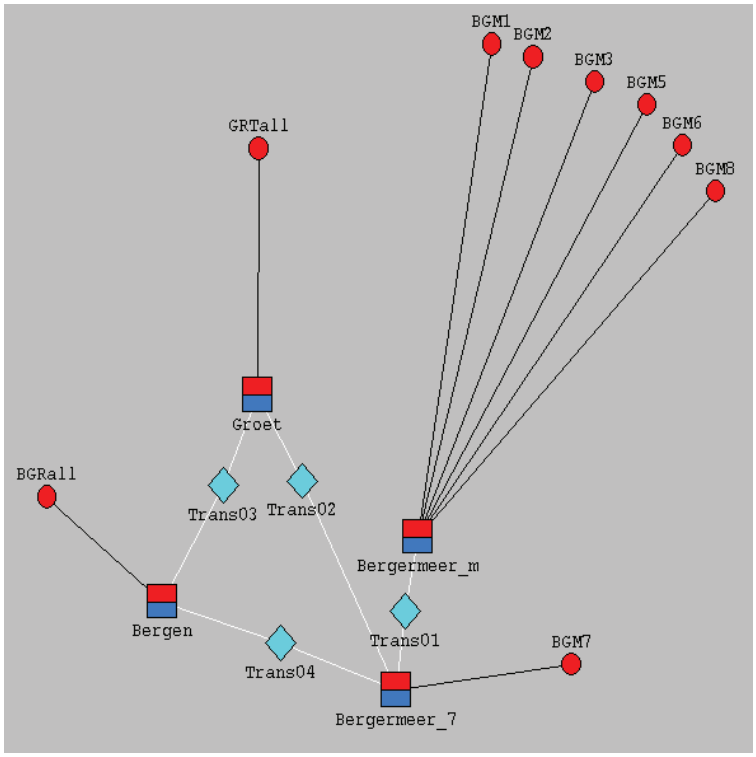

Figure 5-26 **Alternate configuration (compartment volumes corresponding to eastward extension of 'fault2'): GRT communicates (if at all) with BGM7 rather than BGM_main.**

Table 5-12 **Match parameters with BER and GRT connected to BGM_main, rather than BGM7.**

GIIP:

	Bergermeer_main	Bergermeer_7	Bergen	Groet
GIIP (GSm^3)	13.83	4.4	7.85	7.2

Transmissibility:

	Bergermeer_main to Bergermeer_7	Bergermeer_7 to Groet	Bergermeer_7 to Bergen	Groet to Bergen
C (m^3/day*mPa.s/bar)	5.5	0.3	0.06	0

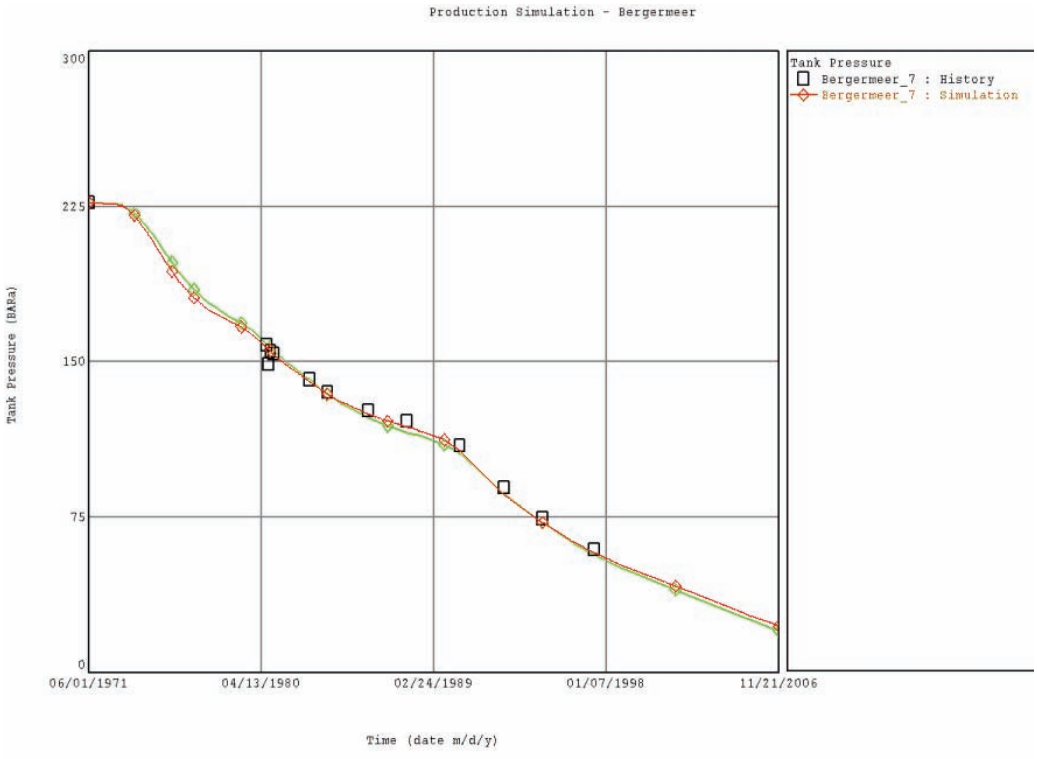

Figure 5-27 **Alternate match of Bergermeer_7, with setup as in Figure 5-26. Red: base; green alternate.**

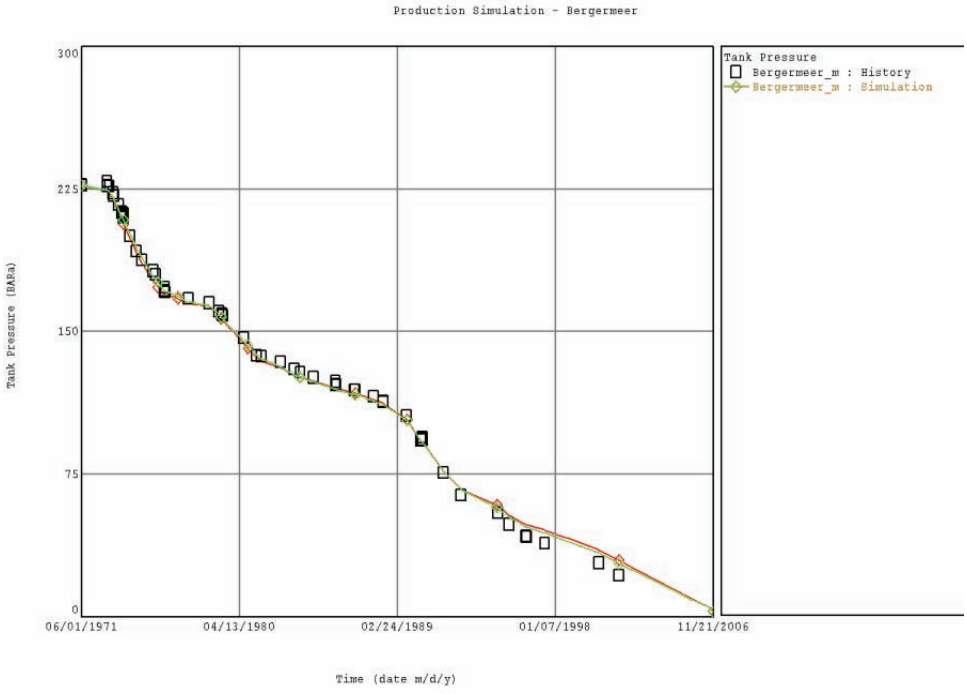

Figure 5-28 **Alternate match of Bergermeer_main, with setup as in Figure 5-26. Red: base; green: alternate.**

5.2.2.4 *Conclusion*

The total GIIP of Bergermeer is fixed with a relatively high degree of accuracy. An uncertainty remains on how this volume is distributed between Bergermeer_main and Bergermeer_7. Sensitivities on inter-block transmissibilities and aquifer strength yielded a volume range for Bergermeer_7 falls from 4 to 7 GSm^3.
The behaviour of the GRT and BER fields makes it unlikely that there is a non-trivial aquifer attached, or that there is significant communication to other fields. In particular the GRT←→BGM transmissibility is an order of magnitude less than the transmissibility between Bergermeer_main and Bergermeer_7.
The pressure behaviour of Bergermeer_7 in particular does allow for some, very limited, aquifer influx.

5.3 Simulation

Dynamic flow simulations were set up using Petrel RE (version 2005.1). They were then run with Eclipse (v2006.1). This ensures a well-defined relationship to the geological model, and minimizes conversion problems. In addition it allows effectively grid-independent model construction.

5.3.1 Upscaling & simulation grid; Adhoc high k_v/k_h scenario

The settings for property upscaling were discussed in chapter 4. Two simulation grids were used: 100mx100m, with 10 and 25 layers. This means that there was no areal upscaling. The 25-layer model has thinner cells, and therefore higher k_v/k_h ratios (Table 5-14).

The 10-layer model was used for most history matching. This was on the one hand more practical (faster runtimes), and also did not affect the contact prediction too much (Figure 5-31). Volumetric parameters have been tuned with the 10-layer model, as was the pressure match. The 25-layer model was used to run checks, on GWC movement and water production in particular, and to verify in the forecasts that e.g. the (potential) gas flow to Groet was not underestimated because of gridding errors.

It should be noted that because we only did vertical upscaling, not horizontal, each gridblock in the dynamic simulation model corresponds to a single stack of geomodel cells (voxels). Thus the geomodel PERM → flow model PERMK upscaling is forced to be harmonic. This implies an assumption on the lateral size of the heterogeneities (i.e. that their extent is (significantly) larger than the gridblock size, 100x100m), which is in approximate agreement with the body/variogram settings chosen in the various scenarios (see chapter 4). In view of the results of the well test analyses, the upscaled k_v/k_h may be too low; therefore this assumption could well be incorrect; possibly typical length scales are lower than even the shortest chosen in the scenarios. Since electronic well test data (section 5.4) came in at a late stage, there was insufficient time left to generate yet another scenario from static modelling, hence we chose to do an *adhoc* generation from the most discontinuous scenario:

PERMX/Y_highkv = 0.75*PERMX/Y_cont_mid + 0.25* PERMZ_cont_mid

PERMZ_highkv = 0.25*PERMX_cont_mid + 0.75* PERMZ_cont_mid

The statistics of this scenario are shown in Table 5-16.

The selection of the simulation area of interest (BER, GRT, BGM or BGM+GRT) was made at a late stage, by selecting an appropriate active cell indicator array ('ACTNUM'). In this way the various models are ensured to be consistent, and additional blocks can be brought into the simulation easily (Figure 5-32 - Figure 5-34).

No runs were done with the BER field in connection with other fields, as it rapidly turned out that this field shows the least evidence of communication with other blocks, gas or water bearing (viz. low deviations from straight p/z in Figure 5-15, and large pressure differentials to the other fields in Figure 5-17).

Table 5-13 Model parameters.

	10 layers		25 layers	
	# blocks	Typical CPU [sec]	# blocks	Typical CPU [sec]
BGM	11800	40	29500	
GRT	19363	40		
BER	3380	10		
BGM+GRT	36933	200	92334	1000

Table 5-14 Average properties after upscaling, for both 10 and 25 layer models [cont_mid case]. NTG=0.995 in all cases. Averages quoted are arithmetic, prior to application of any multipliers.

	BGM/10	BER/10	GRT/10	BGM/25
Avg. Por	0.203	0.187	0.178	0.200
Avg. PermX	924	527	442	923
Avg. PermY	924	527	442	923
Avg. PermZ	161	142	59	218

Table 5-15 **Average properties after upscaling, for both 10 and 25 layer models [discont_mid case]. NTG=0.995 in all cases. Averages quoted are arithmetic, prior to application of any multipliers. Note that the BER model was not actually run for this case.**

	BGM/10	BER/10	GRT/10	BGM/25
Avg. Por	0.190	0.189	0.189	0.190
Avg. PermX	637	612	611	636
Avg. PermY	637	612	613	637
Avg. PermZ	69	63	72	116

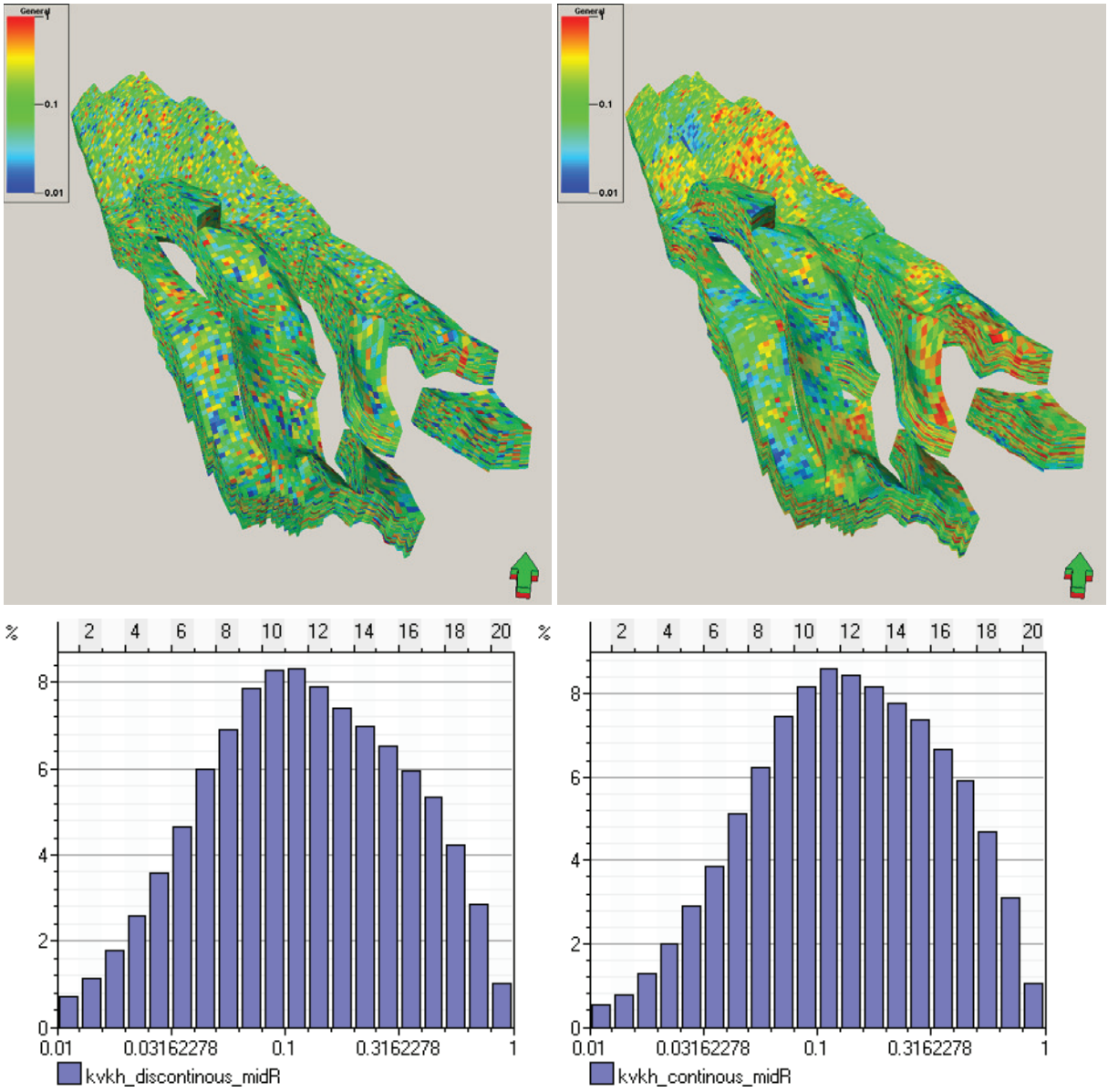

Figure 5-29 **Kv/kh distribution after upscaling, 25 layer model, discont_mid case (left), cont_mid case (right).**

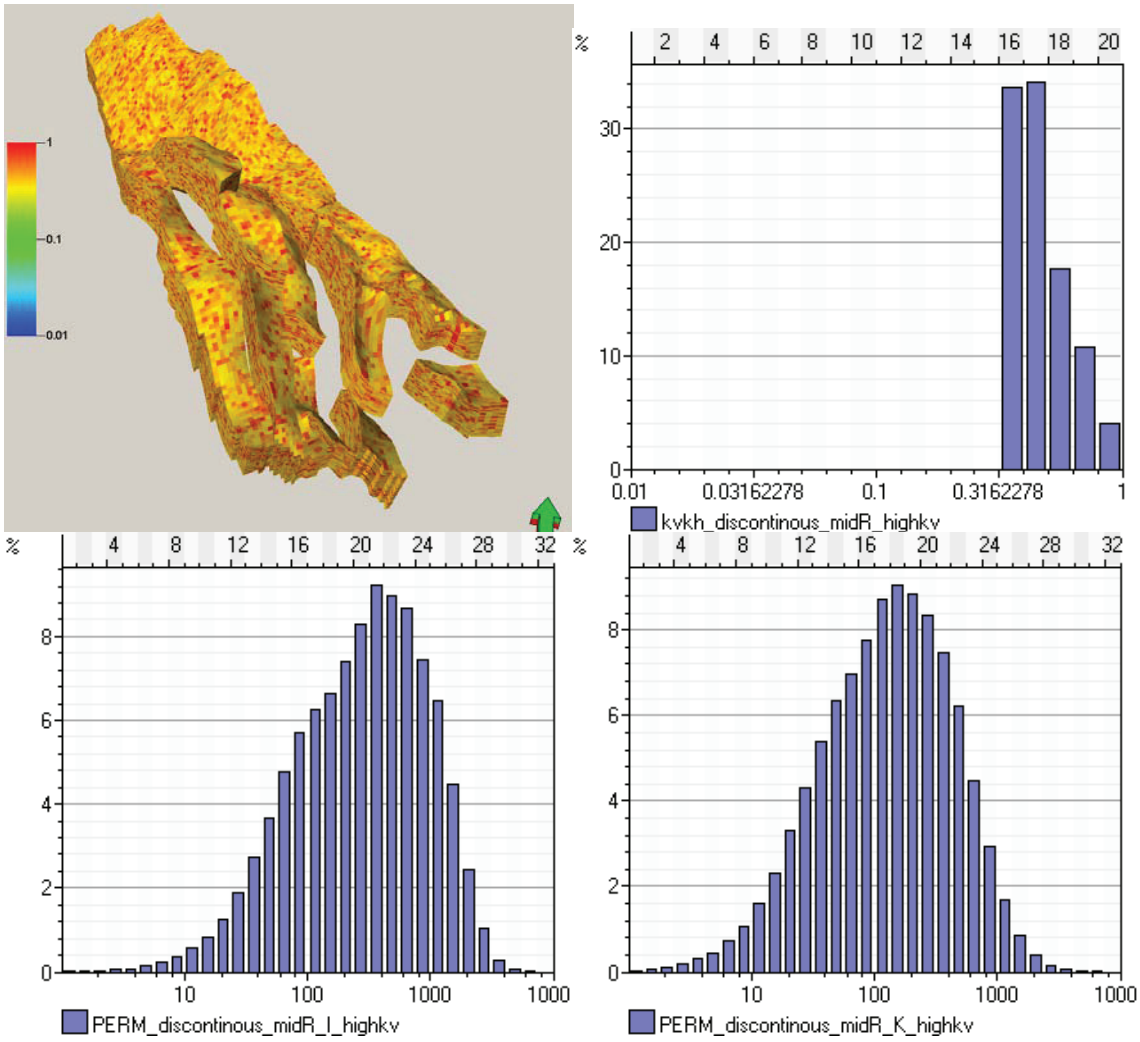

Figure 5-30 **Overview of *adhoc* high kv/kh scenario: 3D plot of k_v/k_h, kv/kh histogram, and k_h and k_v histograms (top left to bottom right).**

Table 5-16 **Average properties after upscaling, for both 10 and 25 layer models [high_kv case]. NTG=0.995 in all cases. Averages quoted are arithmetic, prior to application of any multipliers. Note that the BER model was not actually run for this case. Porosity is as in the 'discont_mid' case from which it was derived.**

	BGM/25	BER/25	GRT/25
Avg. Por	0.190	0.189	0.189
Avg. PermX	506	485	487
Avg. PermY	506	485	488
Avg. PermZ	246	232	305

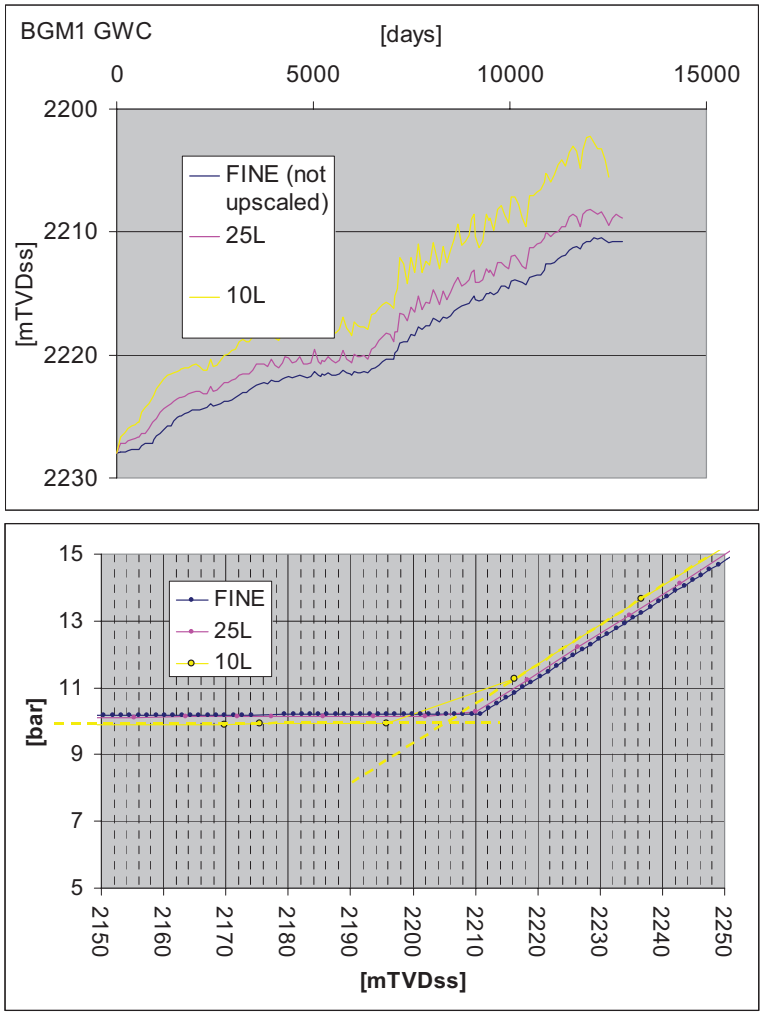

Figure 5-31 **Top: contact movement statistics for a sample 10-layer run and its 25 layer & fine (150 layer) equivalents. The 10-layer run shows a bit more noise and has a tendency to overpredict the rise. The error, however, is at most 5m, well under the gridblock thickness, which means the results match the 25-layer model quite well. The lower plot shows the pressure/height graphs for the three simulations at the final simulation time, illustrating the method (as well as the grid resolution).**

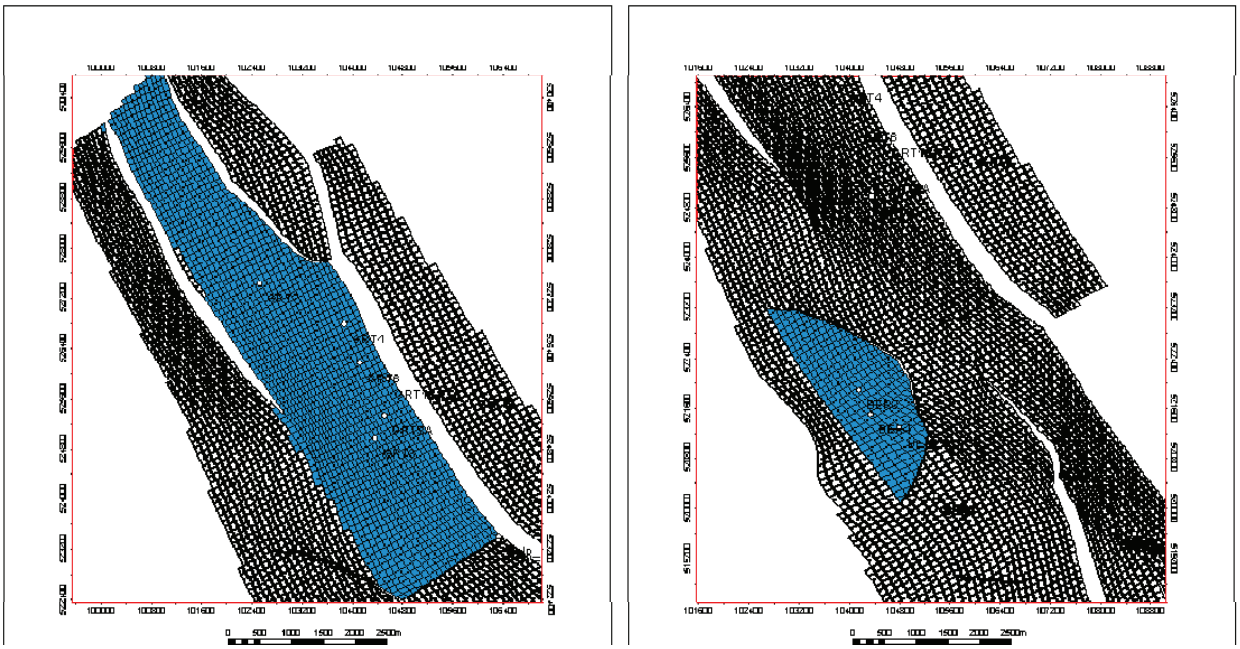

Figure 5-32 Active cells (darker blue) for stand-alone GRT (left) and BER (right) models.

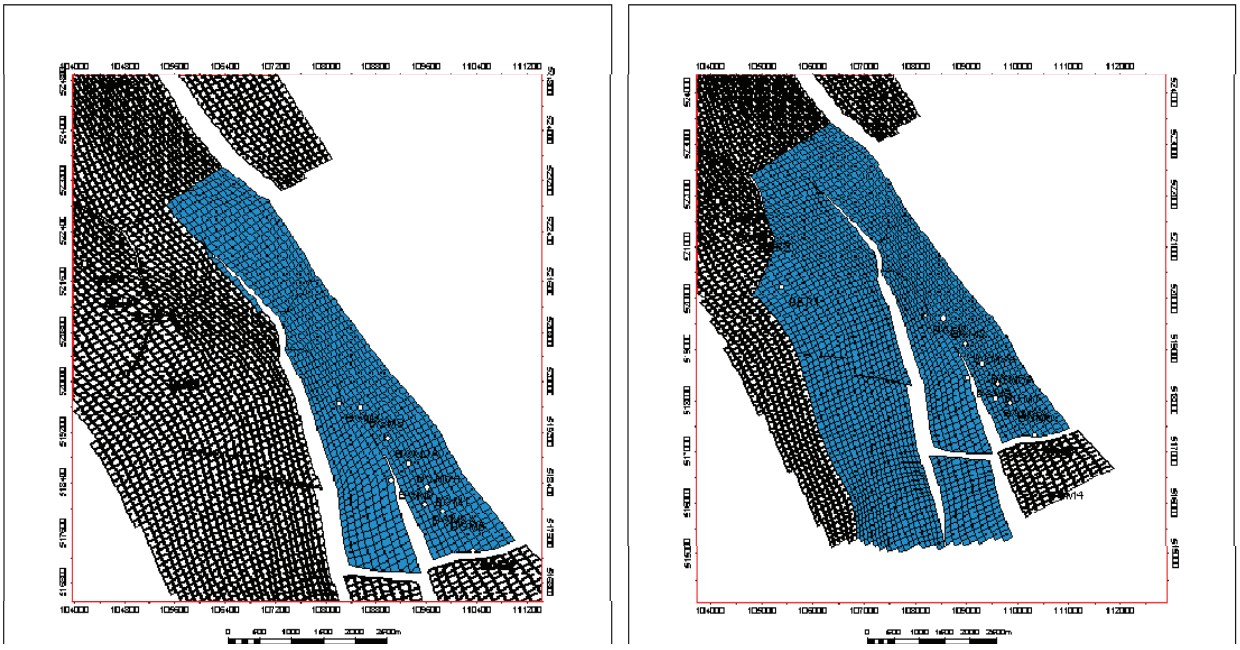

Figure 5-33 Active cells (darker blue) for stand-alone BGM model (left). The right picture shows the active cells for a BGM model with extended water leg.

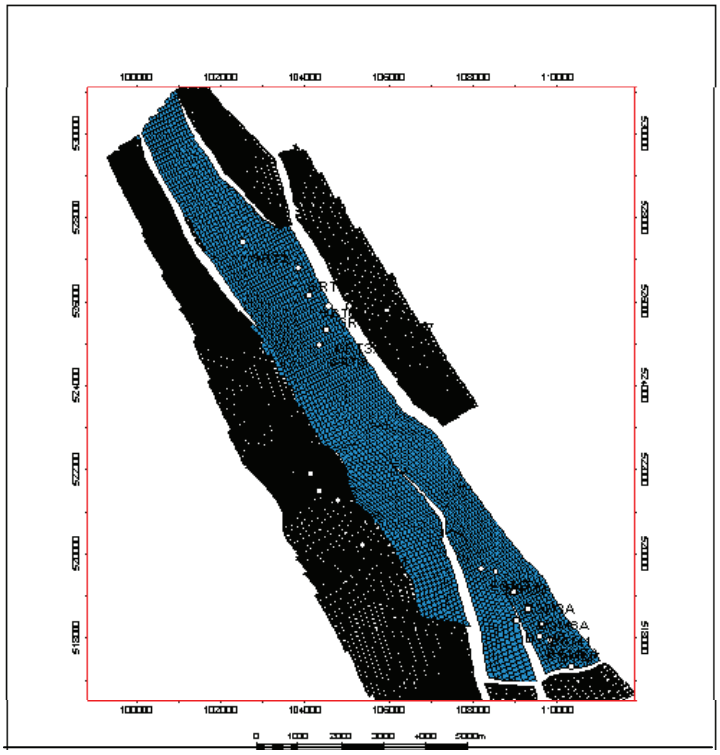

Figure 5-34 Active cells for combined BGM/GRT model.

5.3.2 Adhoc faults

As discussed in the geology chapter 4, there is some uncertainty about faults. From the material balance we conclude that the fields communicate poorly, if at all. However, no faults are apparent from the seismic in the saddle area between in particular GRT and BGM. Moreover, the fault separating BGM_main and BGM7 compartments, which we also can infer from pressure behavior, cannot be tracked all the way on seismic. As we saw in chapter 4, although faulting at the spillpoint is likely, the geology does not unambiguously specifies its nature or location. Similarly, the extension of the fault separating the two compartments is not fixed by seismic or geology.

In the simulation several more or less adhoc faults/fault scenarios have been used, after discussion with the geologists. These are shown in Figure 5-35. The faults (except '2B') follow grid lines (so do not affect the grid). All have zero throw, and are used just for transmissibility multipliers.

It should be emphasized that the decision to introduce them here, after the static modelling, is purely pragmatic. In particular it does not imply that the location of the faults follows clearly from history matching, or other dynamic data. Indeed, as we shall see, it does not, although the dynamic data does present some constraints.

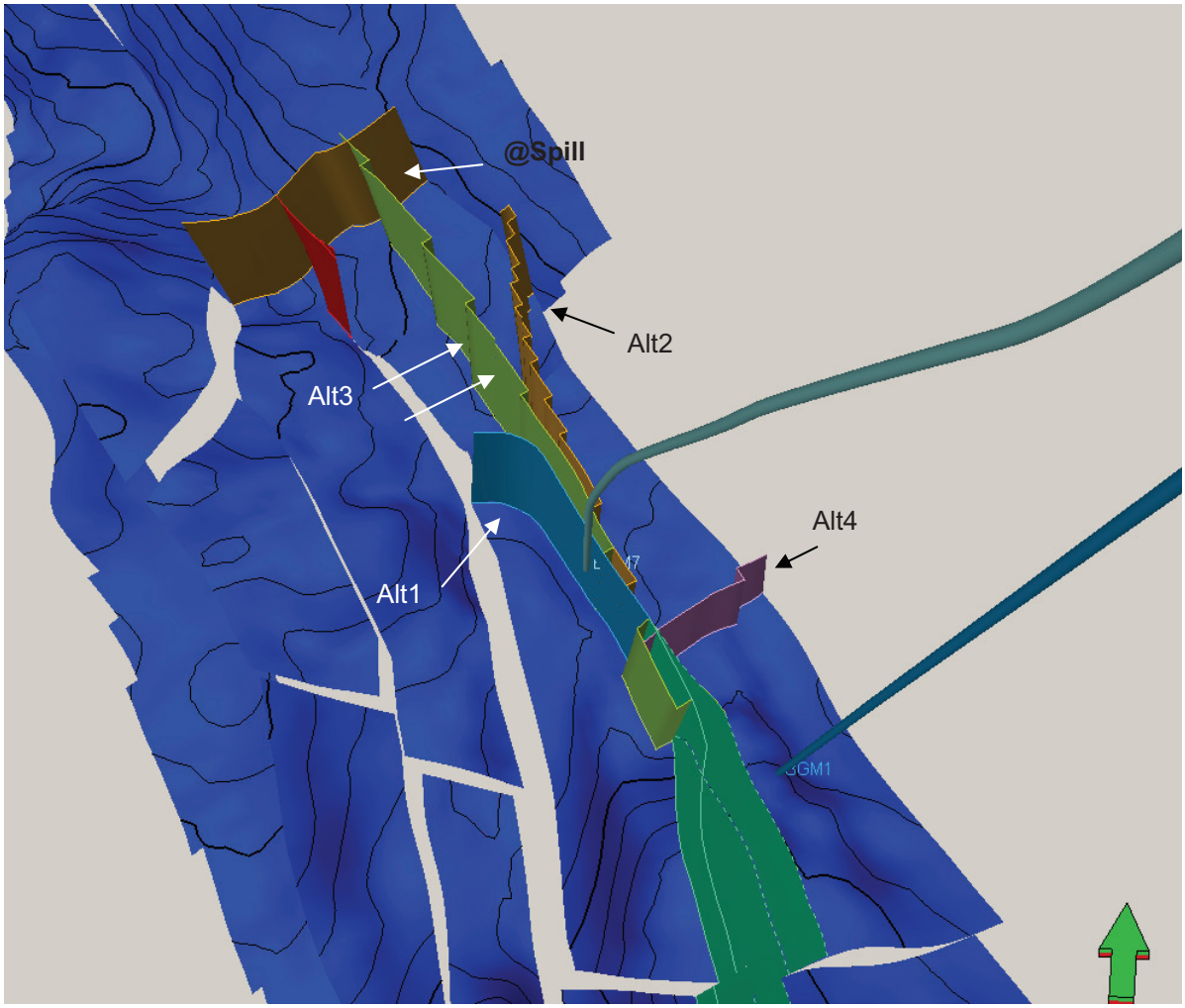

Figure 5-35 **Notional faults in the simulation model introduced where seismic does not indicate faults, but dynamic information does. There is an EW fault across the spillpoint (brown, marked '@ spill'), an extension of the Fault 4 W of BGM7 (red), and four possible extensions of the Fault 2 separating BGM7 and BGM-main (W: '2B', grey/blue; N, '2B alt3', light green; E, '2B alt 2', orange). In addition the most extreme possible (all wells except BGM7 must be in 1 compartiment) E case is plotted ('alt4'). 'Fault2' itself is visible in green.**

5.3.3 Relative permeabilities & capillary pressures

The available data is discussed above (section 5.1.2). The conclusion reached is that S_{gr} does not greatly depend on permeability.

Swc, on the other hand, is fixed by log values, which in the absence of matching the petrophysics to the SCAL)we prefer over the SCAL results. For e.g. BGM1 (chapter 3) the Swc value varies only slightly across the hydrocarbon bearing interval. Since, also more generally, relperm variations within the ROSLU

are not expected to be a major influence (cf. section 5.3.9.5.2), and to avoid adding complexity and parameters to the model, we chose i the base case for a very simplified single model based on Corey coefficients. Different Swc values were used for the different fields (as per chapter 3). Base parameters are shown in Figure 5-36 and Table 5-17. Sensitivities were run to confirm the relative (un)importance of relperm parameters (section 5.3.9.5.2).

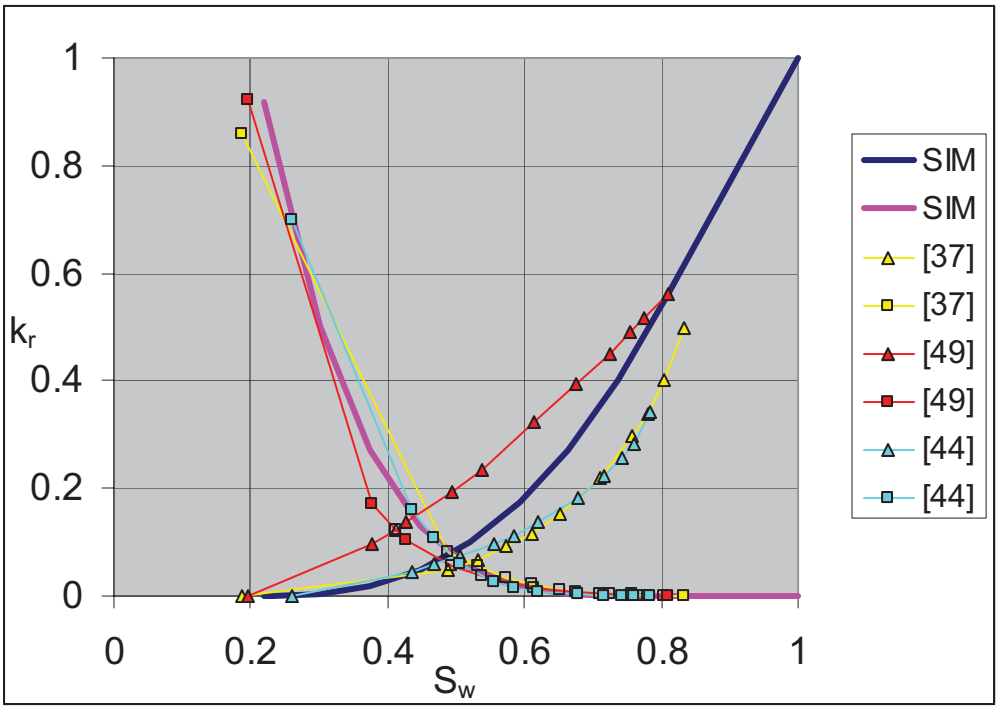

Figure 5-36 **Base BGM relperm curves used in simulation compared to measured curves. [Sample #'s quoted in legend, as in section 5.1.2.] See Table 5-17 for related data. GRT and BER relperms are the same (in the absence of SCAL data for these fields), with different end-points (from well logs).**

Table 5-17 Base relperm coefficients for the three fields in the study.

	BGM	GRT	BER
Swc	0.22	0.34	0.31
Sgr	0.19	0.19	0.19
krg @ Swc	0.92	0.92	0.92
Krw @ Sgr	0.56	0.56	0.56
Corey-w	2.5	2.5	2.5
Corey-g	4	4	4
Krw @ Sw=1	1	1	1

5.3.4 PVT

The gas PVT was input into the simulator as per section 5.1.1 (Figure 5-37). The model used in the simulator is a dry gas model; no condensate production modelling is done.

Other parameters are listed in the table below:

Table 5-18 Non-hydrocarbon PVT parameters. Water parameters are from Petrel RE's default correlation @ 3e5 ppm salinity (which was derived from the apparent water resistivity; chapter 3).

Temperature	86.1 DegC
Water Density @ Surface	1.233 g/cc
Water Formation Volume Factor	1.0266 @ 129.5 bar
Water compressibility	2.86e-5 /bar
Water Viscosity	0.78 cP
Water Viscosibility	0 /bar
Rock compressibility	1e-5 /bar [reversible]

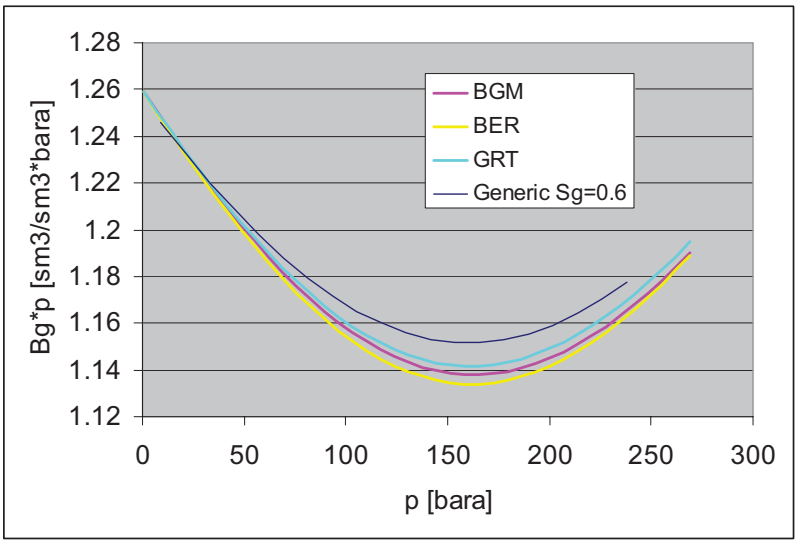

Figure 5-37 Bg vs. pressure for the three fields. For comparison a generic [Petrel RE] S_g-correlation-based curve is added.

5.3.5 Initialization

The initialization of the model is indicated in Figure 5-38. For each of the three fields a contact value is set:

- 2227 mTVDss for BGM,
- 2217 mTVDss for GRT,
- 2150 mTVDss for BER.

Datum pressures are set such that the three fields have identical water pressures (if this would not be the case, we would imply that the fields do not communicate from the outset).

As can be gathered from the graph, this setup does not match all the data properly. In particular GRT is mismatched: initial GRT pressures are *higher* than BGM pressures, but if the contact is as assumed shallower, the pressures should be *lower*. For the purpose of this study (i.e. to be able to investigate whether there can be any communication) we neglected this discrepancy, and tuned the pressures such that BGM is matched.

Also BER does not fit this data exactly, but the discrepancy is less, and the contact cannot be picked so definitely from the logs (chapter 3). Since BER is even less likely to communicate with BGM than GRT, we also neglected this issue.

No transition zones (or capillary pressures) were modelled. In BGM there is little evidence for this being very significant (chapter 3). In GRT this situation is different (log plots in chapter 3 suggest a 40m transition zone), and the transition zone could impact the contact rise. Since, however, GRT was not the main focus of the study, we did not attempt to model this effect.

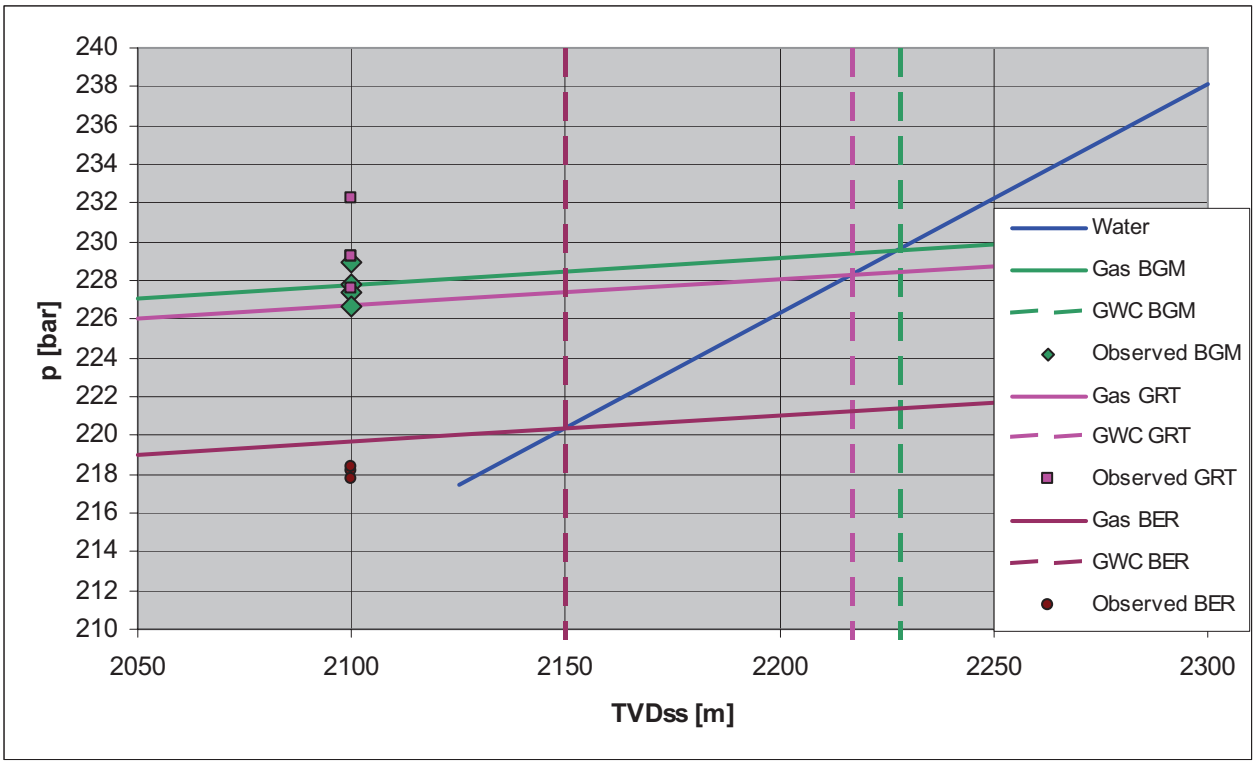

Figure 5-38 **Assumed initialization conditions (contacts) vs. measured initial pressures. The initialization was set such that the Bergermeer field matches the observed initial pressure (green line vs. green points). Given that the aim was to investigate possible communication, BER and GRT must have the same pressure regime as BGM in the water leg (blue line). From this and the initial GWC's, the pressures for BER (brow line & points)and GRT (purple line & points) follow. Both of these are seen not to be an exact match.**

5.3.6 Well Properties

Completion histories were input as per the data provided by Taqa. Zero skin values were used. On the one hand these would not influence the field behaviour modelling. On the other these values change over time [e.g. because of salt precipitation (in GRT), and because of stimulation jobs, see Table 5-8], making an adequate modelling not trivial. Given the main focus of the study (subsurface behaviour) the skin was not considered in the history match (HM). Similarly, in the absence of THP data, no lift curve or THP modelling was attempted in the HM. Both of these are then brought in at the HM→forecast transition to adequately capture well pressure behaviour, as calibrated by test data.

Gas production data, merged with the pressure history, was included as per section 5.1.3. The simulation reports at a resolution of 3 months.

5.3.7 History Match QC's

The plots we used to QC the history match (HM) are mostly standard (and some have appeared above): pressure vs. time or production for the 3 fields (two curves for BGM). In addition we checked water production: although wells were recompleted upward to avoid water production, there was no large water influx during the fields' production history.

It is not expected that this data will fully constrain the model. Hence we did some effort to bring the additional measured data, the GWC rise (Figure 5-10) into the match. This is done by regularly extracting from the model an RFT at the wells where contacts were monitored. From the RFT data the contact can be ascertained. Since the wells are not shut in, the contact is sometimes influenced by near-well pressures. [Note that in order to do this, dummy non-producing equivalents of the wells had to be created. They are "completed" throughout the Rotliegend. Their names start with RFT, to distinguish them from "real" wells".]

The objective of the study was to establish a base for modelling the behavior of the field after conversion to a UGS. To assess the impact of uncertainties that cannot be resolved by history matching on this behavior, we need to prepare a series of "equivalent" matches for representative parameter ranges, and take these forward into the UGS phase to see if they matter. To this end we quantified the HM quality (Table 7-6).

As noted above, the behavior of the field is to a large extent tank-like. Therefore the goal of the "equivalent matches" can only be met if the scenarios we take forward into the UGS forecast are individually GIIP-matched. If we would not do this, behavioural differences would be dominated by the trivial volumetric mismatch, blocking more interesting observations.

To this rule there are some exceptions, as we shall see below (e.g. aquifer) where we intentionally chose parameters for a sensitivity beyond the limits set by the "equivalent" matches constraint, because we felt that imposing the constraint in these cases would make the sensitivity less clear.

5.3.8 Base match

The key match 'knobs' are as follows:

- A pore volume multiplier (MULTPV) fixes GIIP, to match overall pressure decline;
- BGM7→BGM_main fault transmissibility is fixed by matching the initial BGM7 pressure;
- The GRT←→BGM transmissibility is limited by the mid-history GRT pressure match;
- The BGM1 contact rise is matched by (mainly) choosing the permeability multiplier.

No local changes to properties or faults have been made.

The need for accurate volumetrics was shown in the previous section. We have chosen for a more or less phenomenological way, via a pore volume multiplier, because the history match does not actually constrain how the volume deficit (if any) in a given scenario needs to be fixed (structural? property? compartments?).

Rather than engage in speculation, we cut this discussion short and rely on the range of sensitivities treated to be wide enough to cover the possible solutions.

The following comments can be made:

- A good match can be achieved for all three fields in isolation (from each other), without any aquifer.
- The eastward fault scenario has a better match for BGM than the westward. Nevertheless the volumetrics for the BGM7 compartment are still on the low side compared to MBal modelling.
- The pore-volume multiplier needed for BGM (1.14) seems on the high side. The uncertainty in S_{wc} does not seem high enough (a very low S_{wc} would be needed) to explain this. In combination with the previous point, this suggests that there is a possible structural issue. Indeed this is confirmed bt the pore volume multiplier for the structural high case (Table 7-4, section 5.3.9.2) which is below 1. However, the uncertainty map specifies an *envelope* within which we can vary the top surface. Therefore this does not help us in locating the deficit. As argued above, we therefore stay with the pore volume multiplier method.
- The permeabilities, as upscaled, show a k_v/k_h ratio of 0.1 or lower. The HM itself does not constrain.k_v/k_h very well. If we use the k_v/k_h as it results from the upscaling, we need higher permeabilities than suggested by the well test to keep the contact rise under control (see below). Only when the well test data was received and was analyzed, did k_v/k_h become constrained; hence the creation of the *adhoc* high k_v/k_h scenario (see section 5.3.1).

Table 5-19 Main parameters for 'continuous_mid' HM

	BER	GRT	BGM (W fault)	BGM (E fault)	BGM+GRT
MULTPV	1.05	0.95	1.14	1.14	1.14 (BGM) 0.95 (GRT)
MULTX=MULTY MULTZ	1 0.5	0.25 0.125	2 0.5	2 0.5	2 (BGM) 0.25(GRT) 0.5 (BGM) 0.125 (GRT)
MULTFLT 'FaultAtSpill'	-	-	-	-	0.0002
MULTFLT 'Fault2'	-	-	0.0002	0.0002	0.0002
Aquifer	None	None	None	None	None

Table 5-20 **Main parameters for 'high_kv' [based on 'discontinuous_mid'] HM. Note that different pore volume multipliers are needed. This is likely caused by the under-representation of the por trend from BGM to GRT.**

	BGM+GRT
MULTPV	1.22 (BGM) 0.83 (GRT)
MULTX=MULTY MULTZ	1 (BGM) 1(GRT) 1 (BGM) 1 (GRT)
MULTFLT 'FaultAtSpill'	0.0002
MULTFLT 'Fault2'	0.0005
Aquifer	None

5.3.8.1 Bergermeer History Match

As discussed above, the main issues in the BGM history match are:

- BGM7 vs. BGM-main volumes
- BGM7 → BGM-main communication
- Contact behaviour, in particular for BGM1

In the base case match we needed to multiply the overall volumes by 1.14 to obtain a pressure match overall (and to match the material balance analysis). As can be seen from the QC plots, the model with the East trending extension of 'fault2' has a better fit than the West trending variant.

In the as-upscaled models, the contact match is quite reasonable for BGM1, and here also the East trending model does better. To be able to do this, however, we needed to increase the permeabilities somewhat (assuming a 0.5 additional kv/kh multiplier); lower permeabilities lead to increased contact rise This leads to higher permeabilities than the ones estimated from well tests.

Inspecting the 'adhoc high_kv' model has a more or less equivalent pressure match (Figure 5-43), but it does show different contact behaviour (Figure 5-44). The BGM7 measurements are not both naturally matched by either scenario. However, the OH contact that is deeper than the initial BGM GWC could potentially be affected by depth calibration issues; the later TDT measurement is not reinforced by later measurements showing an unambiguous trend (like BGM1).

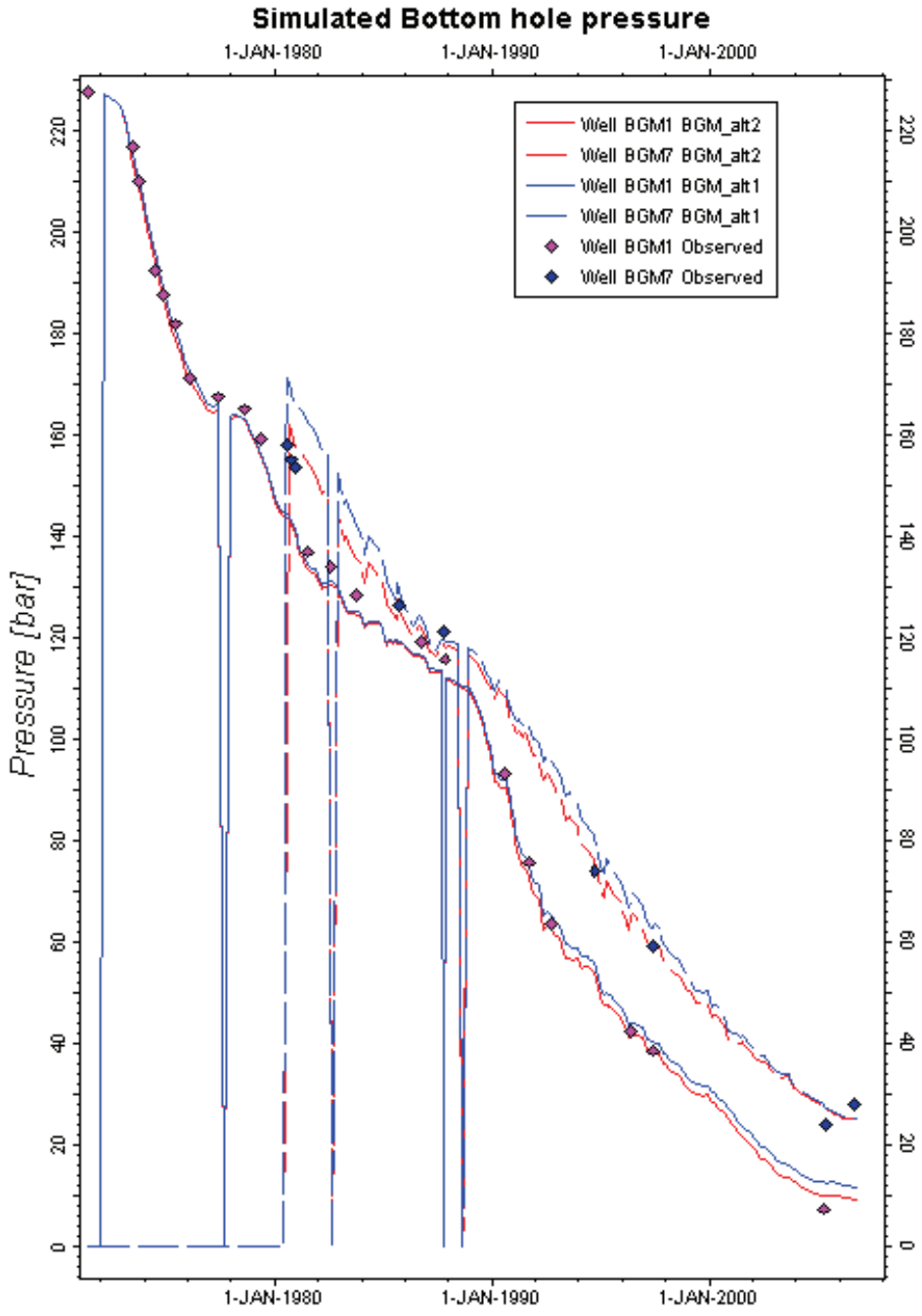

Figure 5-39 BGM 'base' pressure match (left; shown are BGM7 and BGM1. The cases shown are with a W extension of 'fault2' (blue) and a right extension (red). The latter is volumetrically better, and also has a better pressure match.

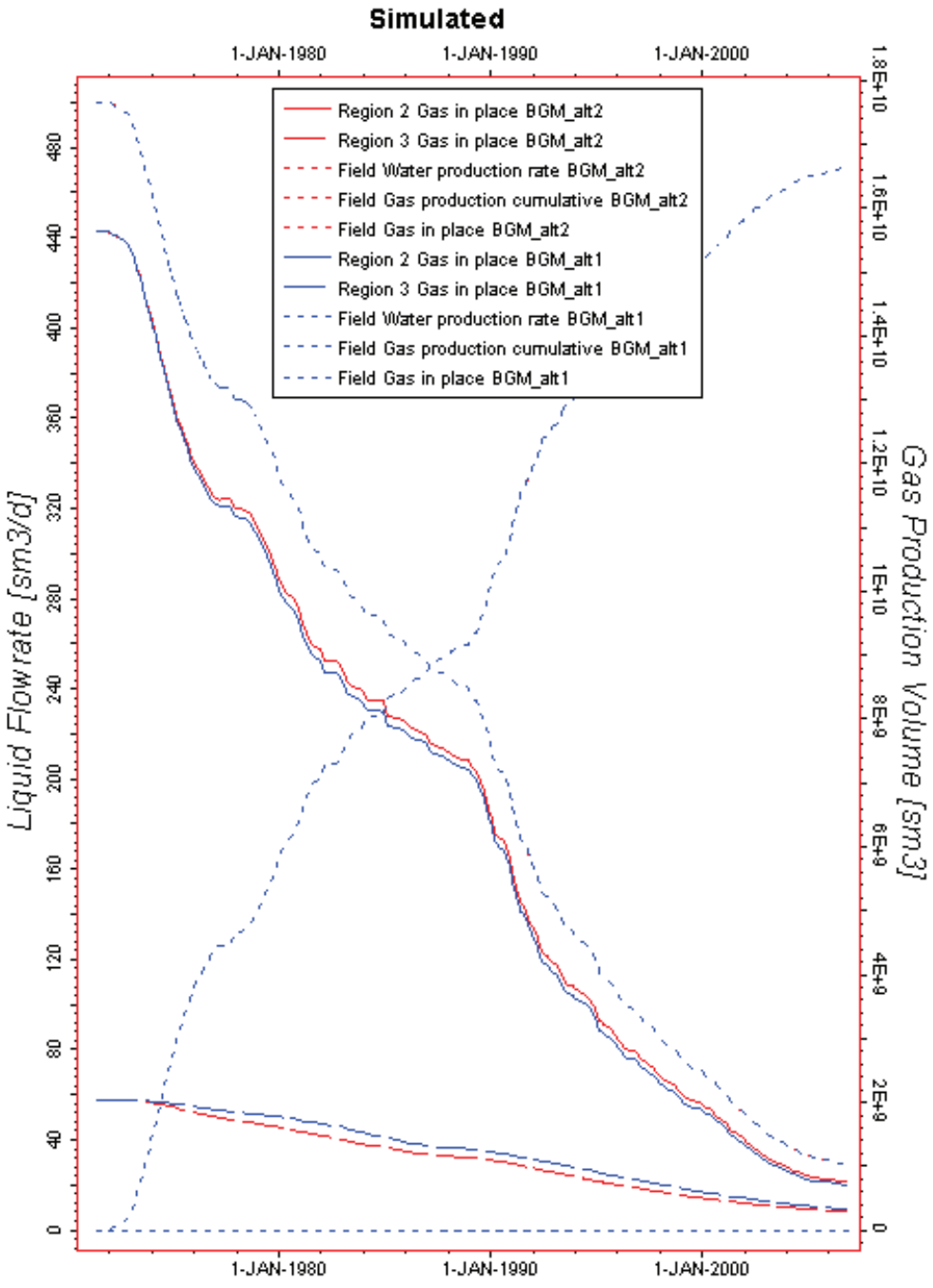

Figure 5-40 BGM 'base' pressure match (left; shown are BGM7 and BGM1. The cases shown are with a W extension of 'fault2' (blue) and a right extension (red). The latter is volumetrically better, and also has a better pressure match.

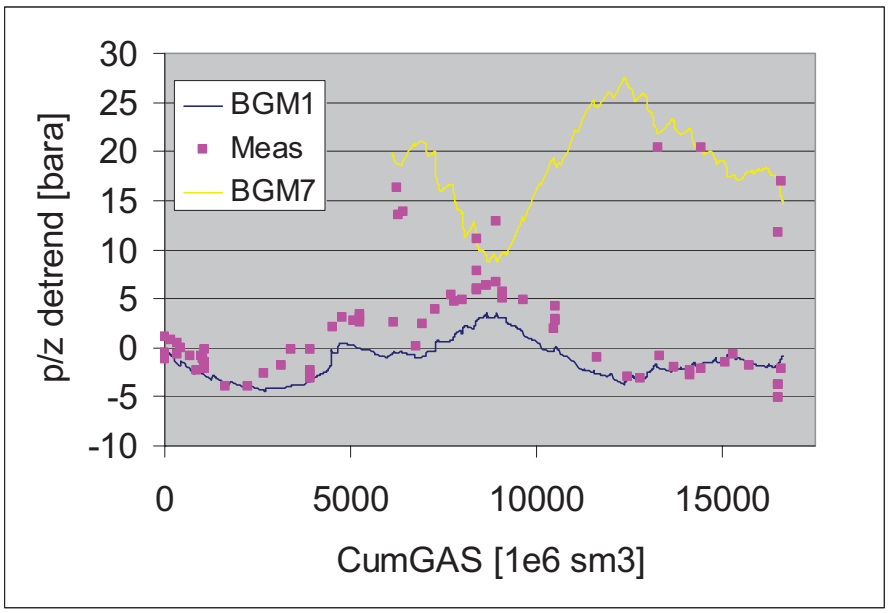

Figure 5-41 **BGM pressure match, zoom-in by plotting detrended (cf. Figure 5-14) [This graph was taken from the 25 layer BGM+GRT model.]**

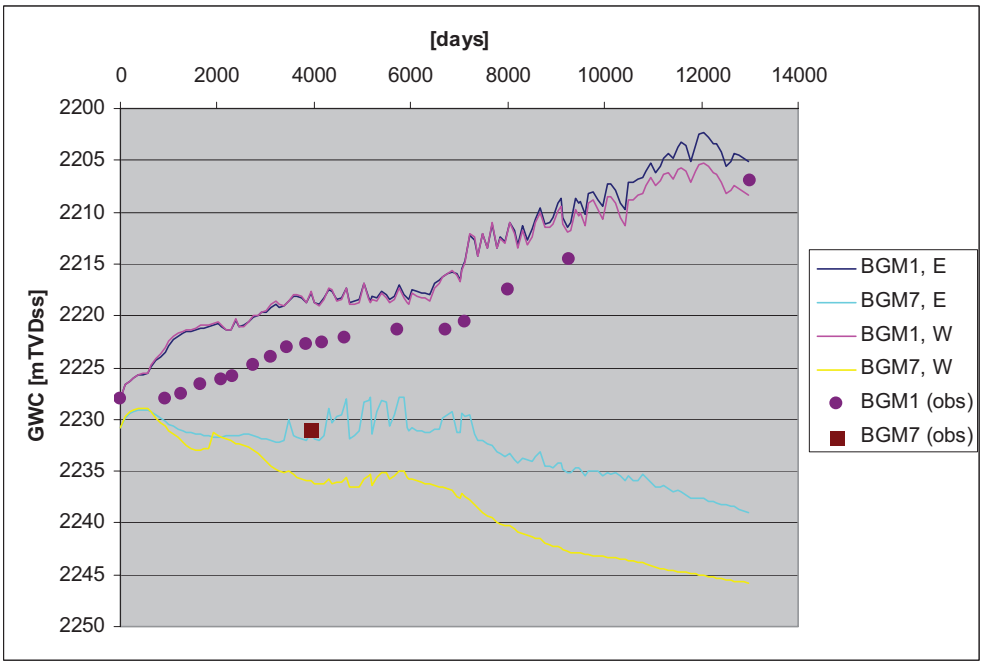

Figure 5-42 **BGM contact match for West extension of 'fault2' (marked 'W') and East extension of 'fault2' (marked 'E').**

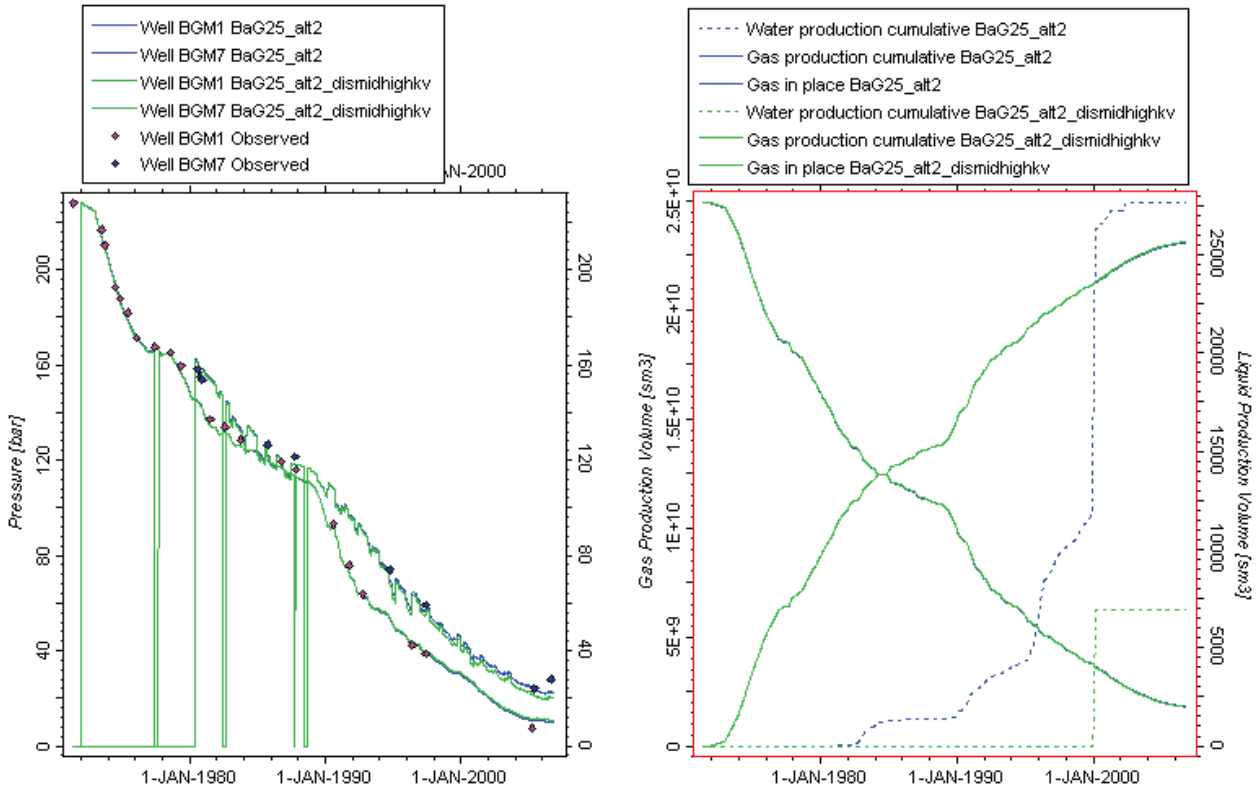

Figure 5-43 **BGM 'adhoc highkv' pressure match (left; shown are BGM7 and BGM1), and region/field volumes, field cumulatives and water production (right). The cases shown (blue: base; green: 'adhoc highkv') are with a E extension of 'fault2', both run on a 25 layer model. Note that they are based on two different property models, which have slightly different amounts of volume in the two compartments. This was corrected for by different pore volume multipliers. The base 25 layer model has a bit of water production, the 'adhoc highkv' has less, corresponding to a slightly less GWC rise.**

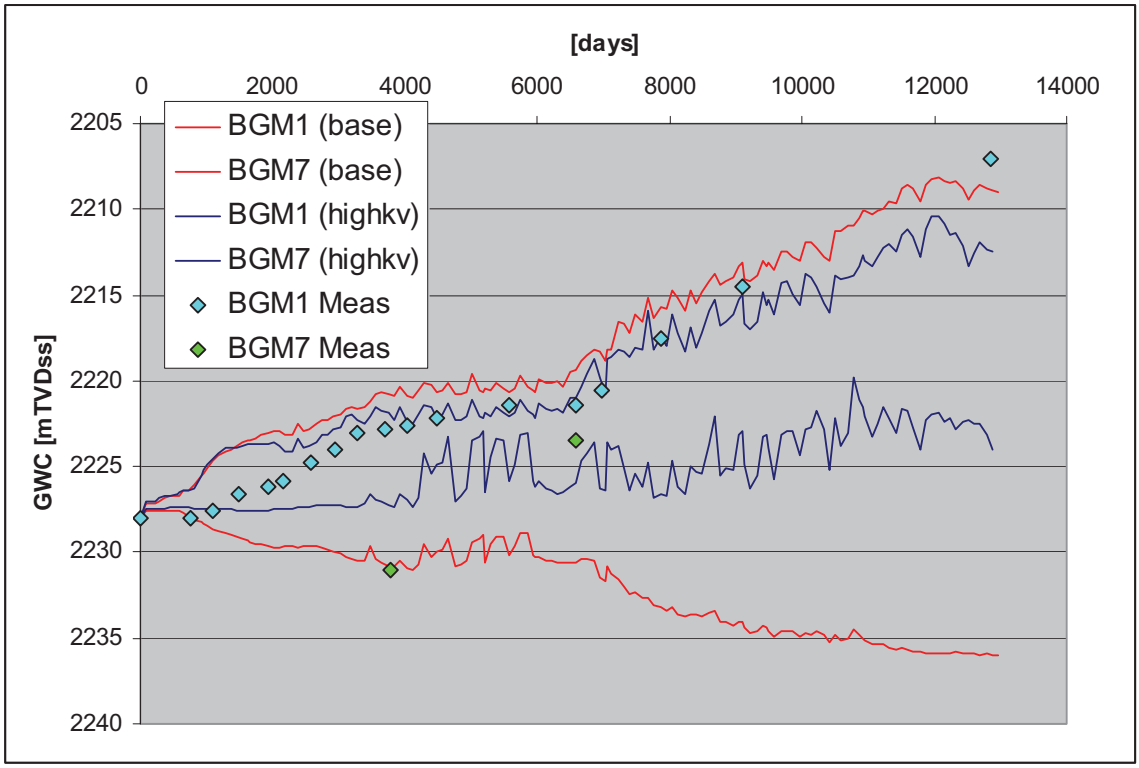

Figure 5-44 **Base ('cont_mid') BGM contact behaviour vs. GWC behaviour in the adhoc high-kv scenario (based on 'discont-mid'). Both are 25-layer models. The property scenario on which the high_kv run is based has a less pronounced 'bell 'permeability profile, which plays a role in the BGM7 contact behaviour in particular. (See the section below on contact dynamics, and Figure 5-48). As regards the BGM1 rise, the difference between the runs is not significant.**

5.3.8.2 Bergermeer contact dynamics

The mechanism for the contact rise, in the absence of an aquifer, is due to a kind of 'collective cone' of the BGM wells. These are eccentrically placed in the field leading to a pressure gradient in the gas. The water responds to this by pushing up the GWC in the well area. Given the relative lack of compressibility in the water leg, and the lack of an aquifer, this can only be achieved by a non-uniform GWC, and this is precisely what happens in the current model. In 'underproduced' parts of the fields, such as the northern part and the BGM7 compartment, the GWC may even go down rather than up.

In order to investigate what the main controls on the model's contact rise mechanism are, we checked it in various sensitivities. Possible factors include:

- Permeability level;

- Kv/kh and/or low scale heterogeneity;
- Large scale vertical heterogeneity ("bell" profile; see chapter 3 & 4).
- Areal heterogeneity (permeability decreasing northward to GRT)
- Compartmentalization

It should be noted that these factors are not independent; the HM constrains them so they are correlated. E.g. the higher the permeability, the more prominent a baffle the 'fault2' must be, to explain the BGM7←→BGM1 pressure difference.

The main control for the BGM1 contact rise is permeability (Figure 5-46). As permeability increases the BGM GWC goes down. The BGM7 contact behaves less uniformly: at high or low permeabilities, it does not change much. At medium-high values, the contact moves down. In no circumstance does the contact go up, like BGM1, for this set of sensitivities. The maps below (Figure 5-45) illustrate this picture: in higher perm cases the fault is the more important factor, and the BGM7 contact goes down, whereas the internal tilt in the BGM-main compartment is limited. In lower perm cases the internal contact gradient in BGM-main is higher, the fault is less prominent, and the BGM7 contact has moved little.

Studying at Figure 5-47, we observe that the main controlling factor in the *difference* between the BGM7 and BGM1 contacts is the bell curve. Because of this profile (which is very pronounced in the 'cont-mid' scenario) in relation to the GWC, the water near BGM7 sees a higher permeability than the gas (Figure 5-50). Thus the water flows more readily. Removing the bell curve will lead to less water moving from BGM7→BGM_main, and thus to less contact descent in BGM7. This is the explanation for the relative lack of GWC descent in BGM7 in the adhoc high_kv scenario (Figure 5-48; Figure 5-51).

The effects of possible aquifers and compressibility will be treated later in somewhat more detail. In short their effect on GWC behaviour is to work against the zero-sum behaviour of the water in the system: the amount of water escape from BGM7 is fixed (follows from permeability and pressure gradient), but this efflux is countered by aquifer influx and rock compaction, respectively, so that the (initial) BGM7 descent is less or absent.

In summary, the factors influencing the contact behaviour are:

- Permeability level;
  Lower permeability leads to larger gradients in the gas cap, thus to larger large-scale GWC gradients. Lower permeability also leads to local "cone"-like effects. Both imply that lower permeability leads to more GWC rise
- Kv/kh and/or low scale heterogeneity;
  These have a limited effect on GWC rise.

- Large scale vertical heterogeneity (“bell” profile; see chapter 3 & 4).
  The bell profile is important in setting the ratio of water/gas flux in response to a pressure gradient, depending on where the GWC is in relation to this profile. Thus it is an important factor in controlling the BGM7 behaviour, and to a lesser degree on BGM1.
- Areal heterogeneity (permeability decreasing northward to GRT)
  This has a limited effect.
- Compartmentalization
  The smaller the BGM_main compartment is, the more the fault has to be open (since more volumes have to come from BGM7, while the pressure difference is fixed by the history). If more gas flows, more water flows as well. Thus, the smaller BGM_main is, the more does the BGM1 contact rise.

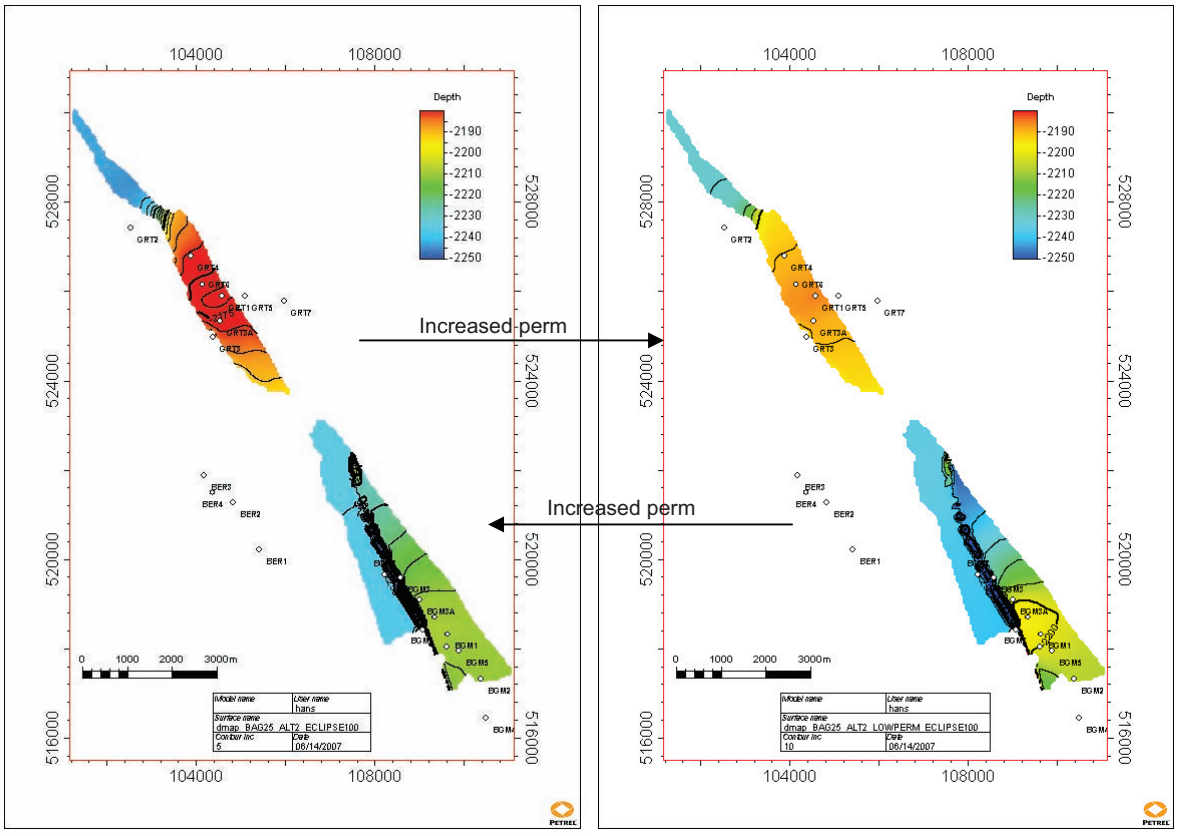

Figure 5-45 **GWC map @ 2005 for two cases: 'cont_mid' base case (left), and a sensitivity of that run with reduced permeability in BGM (right; MULTX=0.5 rather than 2.0). The GRT permeabilities vary in reverse; the multiplier is the same as BGM in the lowperm case (i.e. for GRT MULTX=0.25 on the left, MULTX=0.5 on the right).**

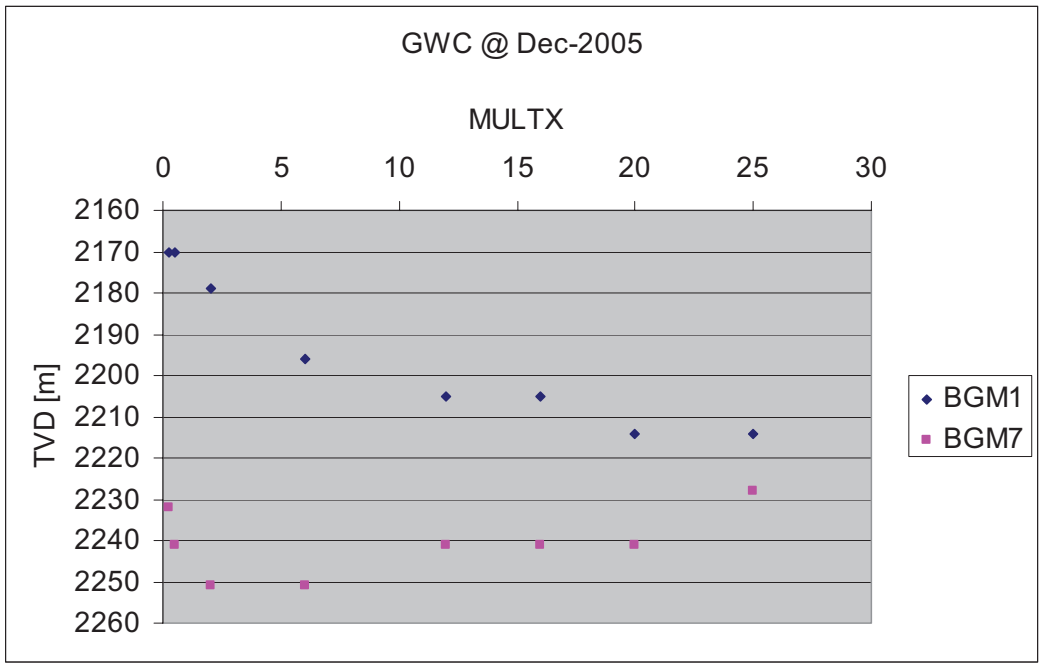

Figure 5-46 **Permeability dependence of the 2005 contacts in BGM7 and BGM1. The x axis shows the x permeability multiplier 'MULTX'. Generally, as permeability increases, the contact tilt as well as the BGM_main/BGM7 difference decreases. At very low permeabilities, the BGM7 contact shows different behavior (coning; cf. Figure 5-51). [Note that these sensitivities were run from an earlier base case than the one presented here; the mechanism is still the same, however, so we chose not to redo these runs.]**

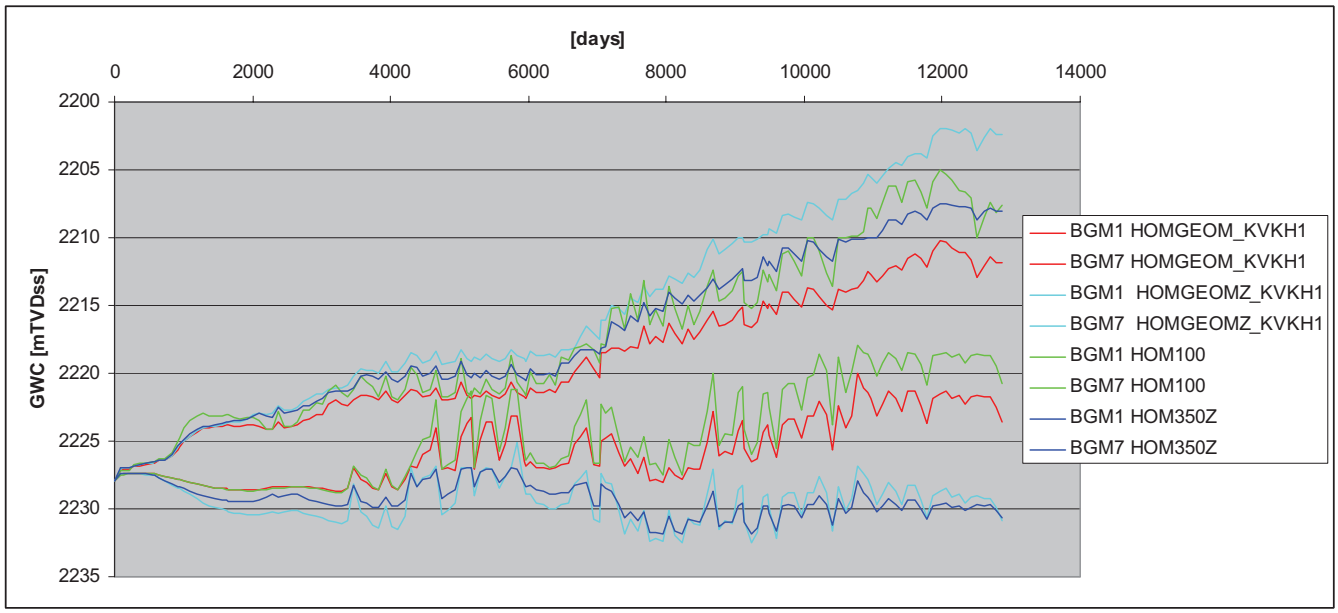

Figure 5-47 BGM1/7 contact movements for various simple permeability scenarios:
HOMGEOM_KVKH1: Permeability from areal geometric average map (of cont_mid), propagated uniformly downward.
HOMGEOMZ_KVKH1: Permeability from areal geometric average map (of cont_mid), propagated downward by multiplication with a simple "bell" profie.
HOM100: Homogeneous, 100 mD
HOM350Z: Homogeneous, 350 mD, multiplied with a vertical "bell" profile.
All runs have kv/kh = 1.

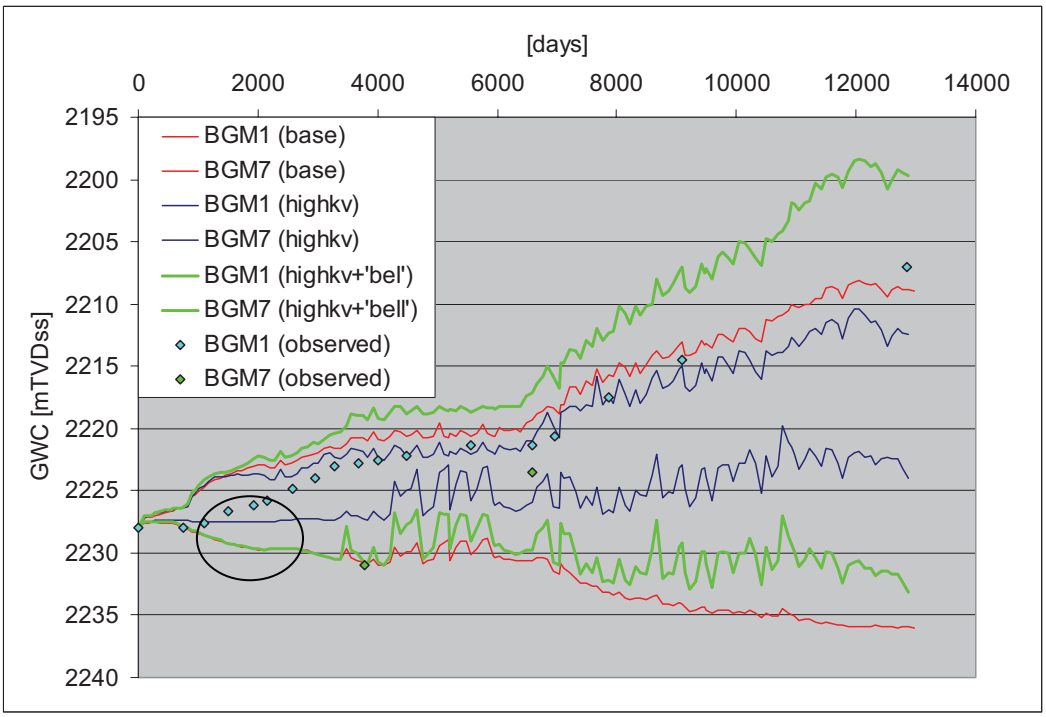

Figure 5-48 **Modification of GWC behaviour if we impose a vertical bell profile on the adhoc high-kv scenario: the initial behaviour of the BGM7 GWC is down, rather than constant. After the BGM7 well comes on production, local effects take over. Also the BGM1 contact is severely affected by the bell profile (permeability levels will have been affected as well).**

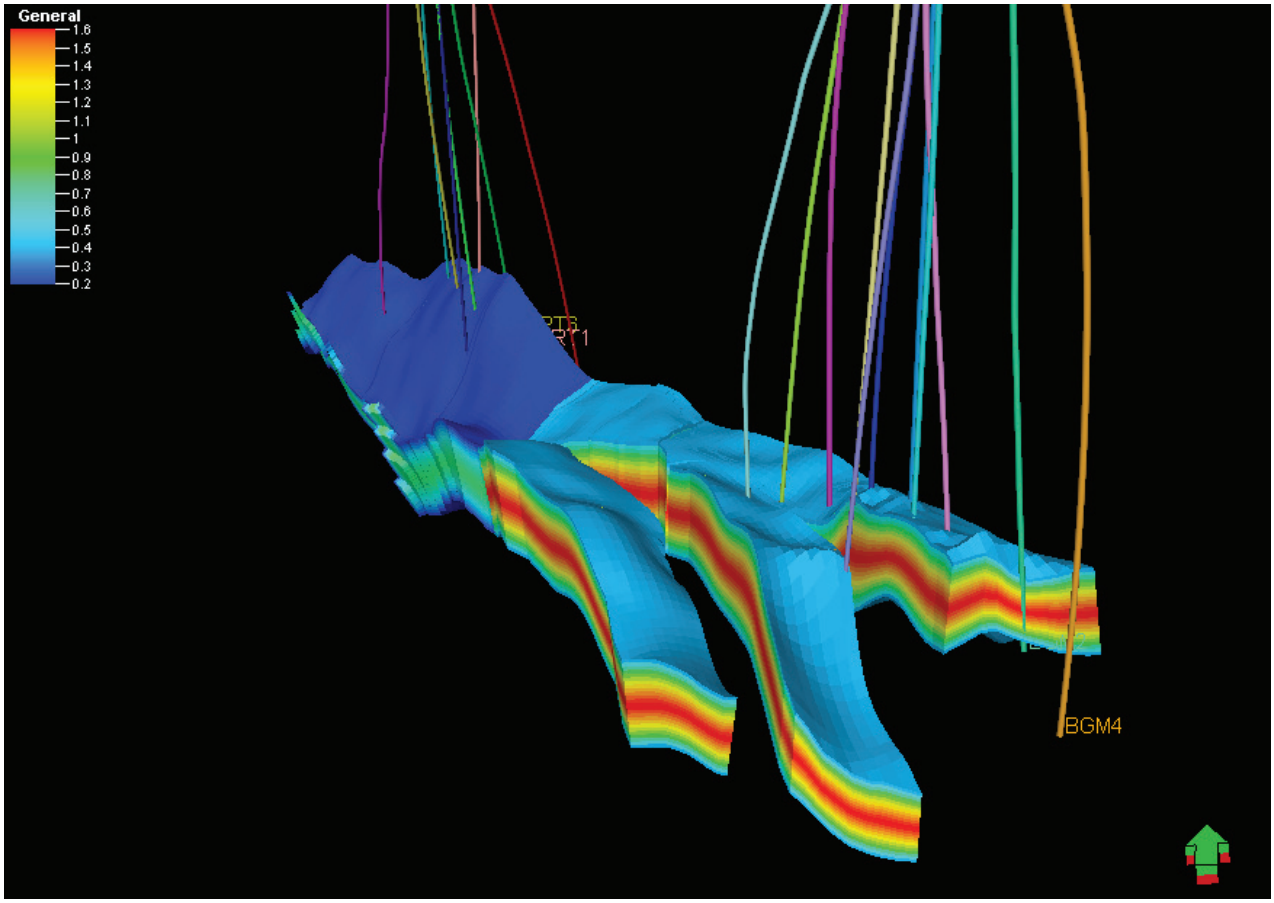

Figure 5-49 **Permeability multiplier (MULTZ=MULTX=MULTY) used to impose 'bell' profile on high-kv run.**

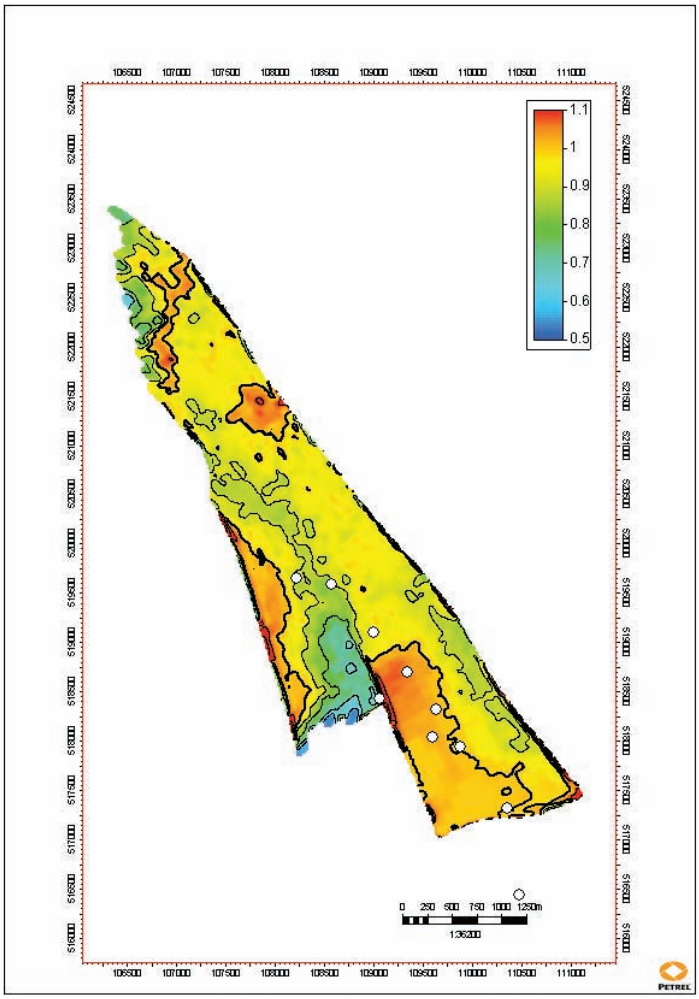

Figure 5-50 **Average permeability above the GWC divided by the average permeability over the full Rotliegend.**

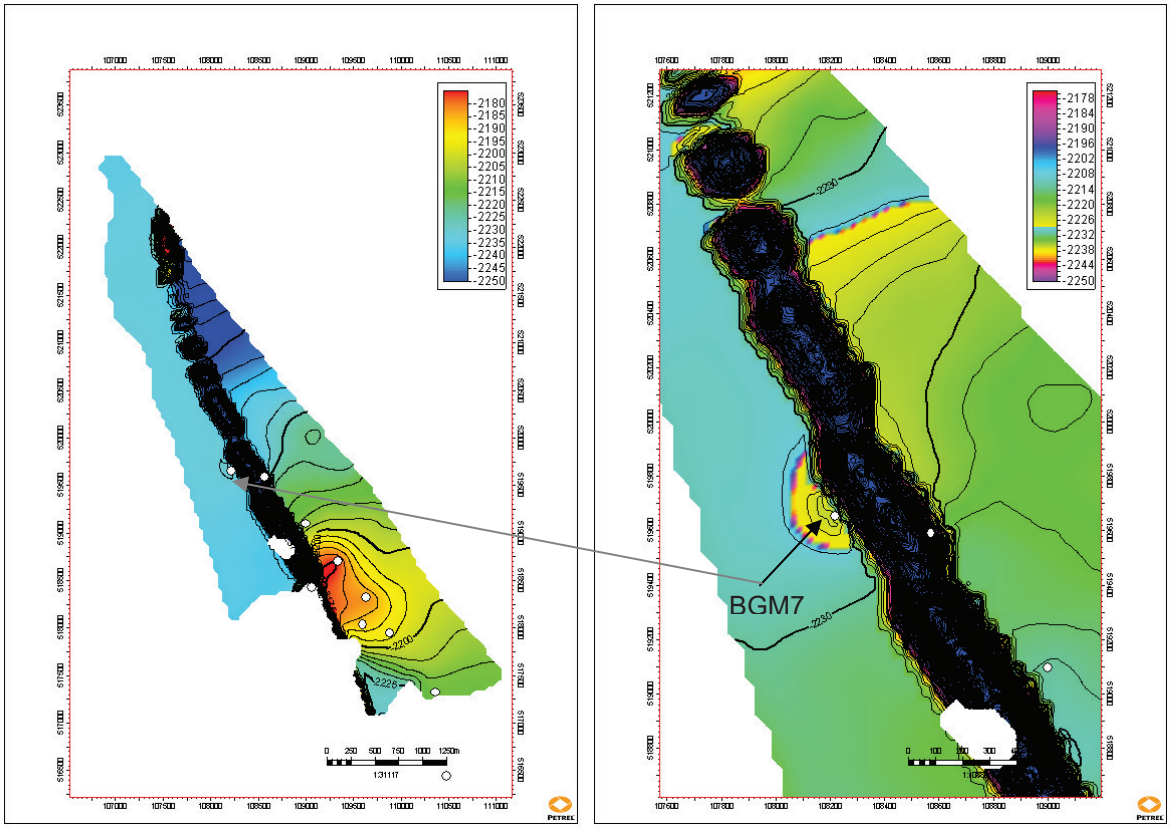

Figure 5-51 **Map of GWC near the simulation end (end 2004) if we impose a vertical bell profile on the adhoc high-kv scenario. The right plot is a zoom-in (different color scale; contours at 2m rather than 5m) showing the local "cone" near BGM7.**

5.3.8.3 Bergen History Match

The Bergen field has the simples HM of the three: only volumetrics is involved. There are no known issues with GWC rise; indeed the model does not exhibit a large rise. Contrary to GRT and BGM, the three BER wells are distributed more or less evenly. Moreover, BER is areally smaller than the other two. For these two reasons no contact heterogeneity can develop.

However, looking at the zoom-in of the pressure match (Figure 5-53), we see that the structure in the deviations from the straight line behaviour are not matched. This non-straight p/z behaviour appears similar to BGM, where it is likely caused by the compartmentalization. Indeed, running a faulted gas cap variation of BER does introduce such behaviour (

Figure 5-54). The conclusion is that, although deviations are rather small, they are significant, and the area of BER whose pressure response we are noticing, is probably compartmentalized. We cannot be really sure, though, whether this fault goes through the gas cap [in the faulted simulation shown, the BER1 block is gas bearing, separated from the BER main block by a baffle]. Since BER is not the main focus, no further work was done along this line.

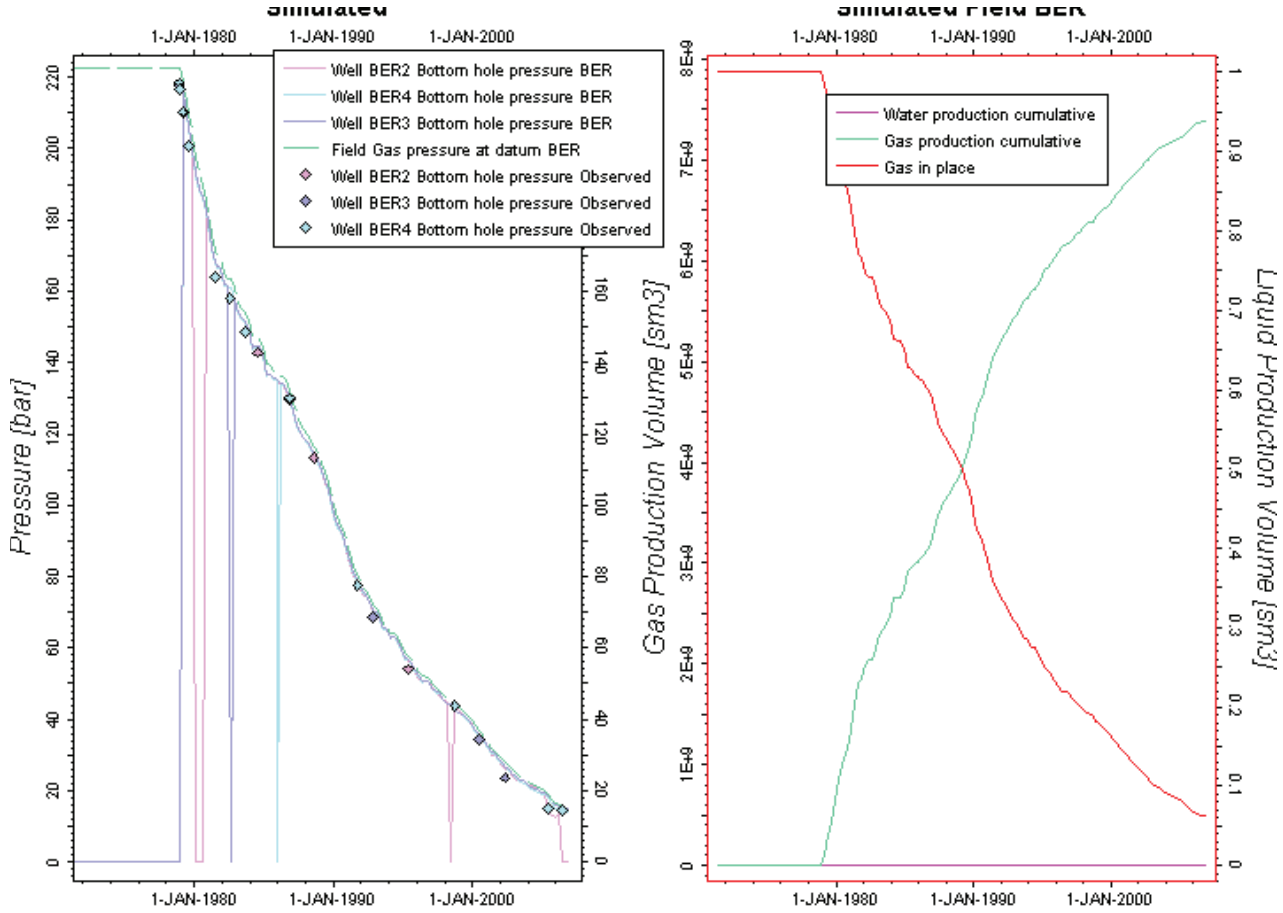

Figure 5-52 **Bergen base pressure match (left) and water production & cumulatives (right). Model water production is zero.**

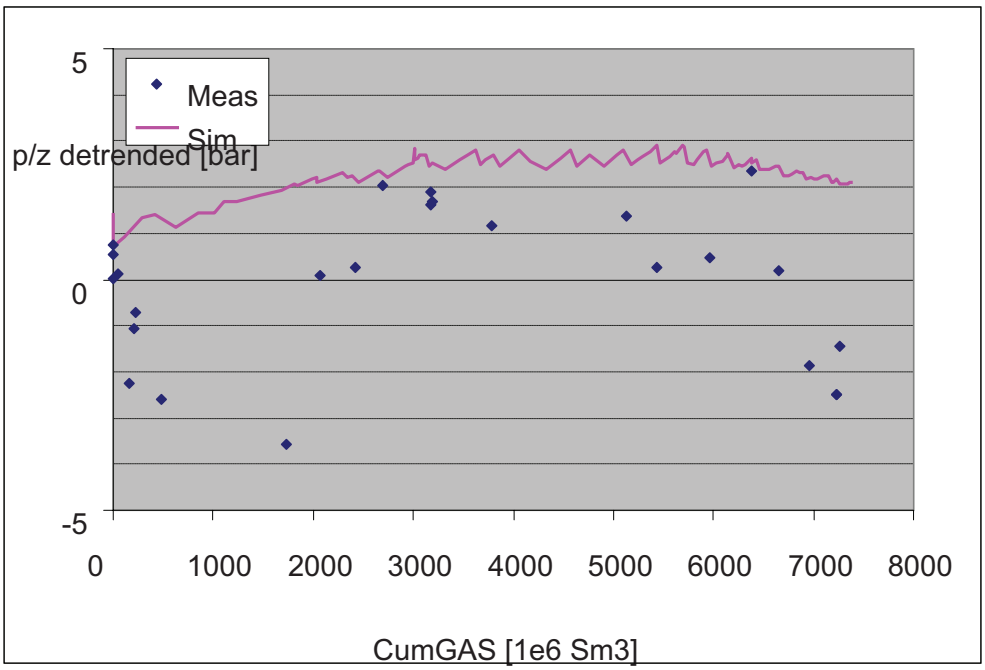

Figure 5-53 BER base case pressure match, zoom-in by plotting detrended (cf. Figure 5-14).

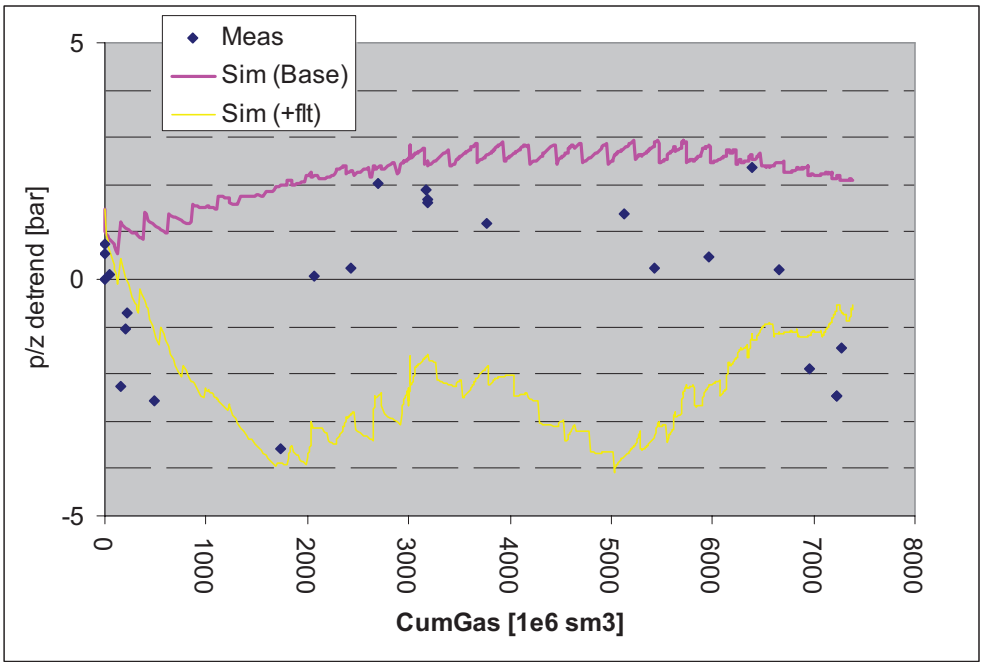

Figure 5-54 BER compartmentalized pressure match, zoom-in by plotting detrended (cf. Figure 5-14). The model also included the BER1 block, since assuming the fault to BER1is not sealing implies that the BER1 block is hydrocarbon bearing. Hence we also needed a different pore volume multiplier for the faulted BER case.
No exact match was intended; the point is merely to show that a multi-compartment BER run shows qualitatively similar behavior to that observed in the BER field.

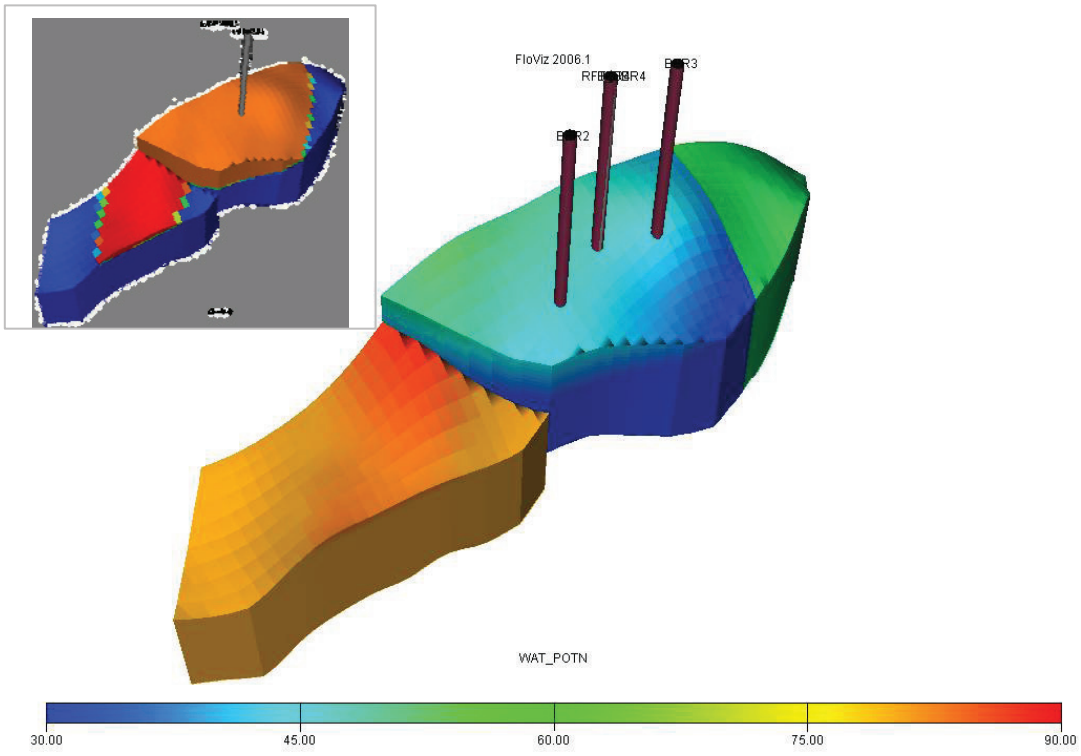

Figure 5-55 **Faulted BER scenario, water potentials at end. The BER1 block is switched on, the connected fault is baffling (thus BER1 is initially gas bearing, see top-left inset, showing initial gas saturations). One additional fault is introduced; this is not meant to be realistic, but just serves to create roughly right-sized compartments.**